LBL-32501
UC-413
Preprint

Lawrence Berkeley Laboratory
UNIVERSITY OF CALIFORNIA

Submitted to Physical Review C

Relativistic Thomas–Fermi Calculations of Finite Nuclei Including Quantum Corrections

D. Von-Eiff and M.K. Weigel

June 1992

| LOAN COPY |
|Circulates |
|for 4 weeks| Bldg. 50 Library.
LBL-32501
Copy 2

Prepared for the U.S. Department of Energy under Contract Number DE-AC03-76SF00098

DISCLAIMER

This document was prepared as an account of work sponsored by the United States Government. Neither the United States Government nor any agency thereof, nor The Regents of the University of California, nor any of their employees, makes any warranty, express or implied, or assumes any legal liability or responsibility for the accuracy, completeness, or usefulness of any information, apparatus, product, or process disclosed, or represents that its use would not infringe privately owned rights. Reference herein to any specific commercial product, process, or service by its trade name, trademark, manufacturer, or otherwise, does not necessarily constitute or imply its endorsement, recommendation, or favoring by the United States Government or any agency thereof, or The Regents of the University of California. The views and opinions of authors expressed herein do not necessarily state or reflect those of the United States Government or any agency thereof or The Regents of the University of California and shall not be used for advertising or product endorsement purposes.

Lawrence Berkeley Laboratory is an equal opportunity employer.

DISCLAIMER

This document was prepared as an account of work sponsored by the United States Government. While this document is believed to contain correct information, neither the United States Government nor any agency thereof, nor the Regents of the University of California, nor any of their employees, makes any warranty, express or implied, or assumes any legal responsibility for the accuracy, completeness, or usefulness of any information, apparatus, product, or process disclosed, or represents that its use would not infringe privately owned rights. Reference herein to any specific commercial product, process, or service by its trade name, trademark, manufacturer, or otherwise, does not necessarily constitute or imply its endorsement, recommendation, or favoring by the United States Government or any agency thereof, or the Regents of the University of California. The views and opinions of authors expressed herein do not necessarily state or reflect those of the United States Government or any agency thereof or the Regents of the University of California.

LBL–32501

Relativistic Thomas–Fermi Calculations Of Finite Nuclei Including Quantum Corrections *

D. Von-Eiff † and M.K. Weigel ‡

June 25, 1992

Nuclear Science Division
Mailstop 70A–3307
Lawrence Berkeley Laboratory
University of California
Berkeley, California 94720, U.S.A.

PACS numbers: 21.60.-n, 21.10.Dr, 21.10.Ft, 21.10.Gv

*This work was supported by the Director, Office of Energy Research, Office of High Energy and Nuclear Physics, Division of Nuclear Physics, of the U.S. Department of Energy under Contract DE–AC03–76SF00098, and the Deutscher Akademischer Austauschdienst (DAAD).

†DAAD fellow. Permanent address: Sektion Physik der Ludwig–Maximilians–Universität München, Theresienstraße 37/III, W–8000 München 2, Bundesrepublik Deutschland.

‡Sektion Physik der Ludwig–Maximilians–Universität München, Am Coulombwall 1, W–8046 Garching, Bundesrepublik Deutschland

Relativistic Thomas–Fermi Calculations Of Finite Nuclei Including Quantum Corrections

D. Von-Eiff and M.K. Weigel

Abstract

Relativistic Thomas–Fermi calculations for finite nuclei including quantum corrections up to second order in $\hbar$; i.e. Wigner–Kirkwood– and exchange–corrections, have been performed. A linear σ–ω model is used, in case of exchange–corrected calculations extended by π–nucleon and tensor ϱ–nucleon contributions. A detailed discussion of the outcome shows that the inclusion of quantum corrections improves the description of the nuclear surface and the classical forbidden region in comparison to the standard relativistic Thomas–Fermi model. Furthermore, special attention is devoted to the investigation of the spin–orbit interaction and the influence of the σ–meson mass on nuclear properties.

1 Introduction

In recent years the interest in the investigation of nuclear systems has shifted strongly towards a relativistic approach (see, for instance, Refs. [1, 2]). The Walecka model (for a review, see Ref. [1]) and its extension by Boguta and Bodmer [3], who added nonlinear contributions through cubic and quartic terms in the scalar field, have been widely and successfully used to describe the ground–state properties of finite systems within the Hartree approximation [1, 4, 5]. More elaborated and fundamental models, like Dirac–Hartree–Fock [6] or Dirac–Brueckner–Hartree–Fock [7, 8], which moreover use more sophisticated Lagrangians, have also been investigated.

However, most of these applications are quite involved, because the evaluation of energies and density distributions demands the knowledge of the wavefunctions of all occupied single–particle states. This can be circumvented by means of semiclassical methods. They allow the study of average nuclear properties in a systematic and transparent way, while the task of calculating the wave functions is avoided, which simplifies the numerical treatment enormously. Within the simplest semiclassical approach, namely the Thomas–Fermi approximation, the Walecka model has been solved for finite nuclei by several authors [1, 9–11].

Semiclassical models including higher order corrections have been used with great success in *nonrelativistic* nuclear physics (see, for instance, [12, 13]). These models are commonly based on the Wigner–Kirkwood (WK) $\hbar$–expansion [14] of the phase–space density, whose lowest order corresponds to the Thomas–Fermi approximation.

Quite recently, several groups have begun to apply semiclassical methods including WK–corrections to *relativistic* problems. Due to the matrix structure of the relativistic Hamiltonian, the task of performing the $\hbar$–expansion of the density matrix is much more involved [15–19]. Using this scheme to describe nuclear systems whose potential has to be determined selfconsistently, e.g. within the (non–)linear σ–ω model, one faces two crucial problems: firstly, the particle– and energy densities including WK–corrections up to second order in $\hbar$ are complicated functionals of the meson–fields, their first and second derivatives and the Fermi momenta. To our knowledge, the problem of a *selfconsistent* WK–approach has not yet been solved in the nuclear context. The second problem is the well known fact that the WK–corrections in coordinate space diverge at the classical turning point. Krivine et.al. [20]

pointed out that these are distributions rather than functions in the mathematical sense and can only be used for the computation of expectation values of one body operators but not for the determination of r–space densities of any kind to improve shapes predicted by Thomas–Fermi calculations.

Both of these problems can be overcome by the density functional formalism, in which the scalar– and time–like potentials and their derivatives are eliminated in favour of the corresponding densities and their derivatives. The basic theorem of Hohenberg and Kohn was extended to Quantum Hadrodynamics (QHD) for the Walecka Lagrangian by Speicher, Dreizler and Engel [19], thus providing the theoretical foundation of the approach. Numerical investigations within nonlinear σ–ω models were carried out by Centelles et.al. [21, 22].

However, the density functional approach is not equivalent to the WK–approach, because they originate from different arrangements of the $\hbar$–expansion of the energy functional. This is illustrated in Ref. [22] for the case of a given external potential, namely a relativistic harmonic oscillator: while it can be numerically shown that the WK–results up to second order in $\hbar$ are equivalent to those obtained by the Strutinsky averaging method, which uses single–particle occupation numbers smoothed by some averaging function to seperate the smooth part of the energy from the fluctuating shell corrections [23], the density functional approach yields different results. It has been shown in the nonrelativistic case that these discrepancies increase within selfconsistent calculations [24]. Hence, the rearrangement of the $\hbar$–expansion causes some "loss of information", which in turn results in a not so proper estimation of the smooth part of the energy by the density functional approach. The specific nature of this "loss of information" is one of the questions that we address in this paper.

Like the WK–corrections, exchange–(Fock–)terms are quantal corrections of the order $\hbar^2$ [17]. Hence, dealing with quantum corrections up to the second order, both kinds of corrections have to be taken into account. Furthermore, exchange–corrections allow the study of π–meson and tensor ϱ–nucleon contributions to nuclear properties. A semiclassical treatment of such more realistic Lagrangians as used in relativistic Hartree–Fock (RHF) or Brueckner–Hartree–Fock (RBHF) calculations seems to be a meaningful task, since even the RBHF–approach can be parametrized in a RHF–structure by means of density dependent coupling constants [25, 26].

For all these reasons, we considered it worthwhile to perform semiclassical

calculations of finite nuclei including both quantum corrections up to second order in $\hbar$. They are taken into account in a kind of perturbative treatment as outlined in section 3. Their impact on average nuclear properties is studied in a systematic way; special attention is devoted to the strength of the spin–orbit interaction, the description of the nuclear surface and the influence of the σ–meson mass on nuclear properties.

The paper is organized as follows. In section 2 the expressions of the relativistic Thomas–Fermi approximation (RTFA) within a Walecka model are recalled. The way we incorporated the WK– and exchange–corrections in our calculations is described in section 3. Section 4 contains the results and their discussion. Our conclusions are drawn in section 5. To complete the paper, we give in the Appendix the explicit expressions for the second order WK–corrections to the various densities.

2 Relativistic Thomas–Fermi Approximation (RTFA)

For the sake of completeness we recall briefly the expressions of the relativistic Thomas–Fermi description of finite nuclei within a Walecka model [1]. The dynamics of the nuclear system are governed by the following Lagrangian, including the electromagnetic field and ϱ–meson contributions to take proton–neutron asymmetry effects into account (we use the units $\hbar = c = 1$):

$$\mathcal{L}_1 = \mathcal{L}_N^0 + \sum_{M=\sigma,\omega,\varrho,A} \left[\mathcal{L}_M^0 + \mathcal{L}_{MN}\right] \tag{2.1}$$

with the free nucleon– and meson–Lagrangians

$$\mathcal{L}_N^0(x) = \bar{\psi}(x)\left(i\gamma_\mu\partial^\mu - M\right)\psi(x), \tag{2.2}$$

$$\mathcal{L}_\sigma^0(x) = \frac{1}{2}\left(\partial_\mu\varphi(x)\partial^\mu\varphi(x) - m_\sigma^2\varphi^2(x)\right), \tag{2.3}$$

$$\mathcal{L}_\omega^0(x) = \frac{1}{2}m_\omega^2\omega_\mu(x)\omega^\mu(x) - \frac{1}{4}F_{\mu\nu}(x)F^{\mu\nu}(x), \tag{2.4}$$

$$\mathcal{L}_\varrho^0(x) = \frac{1}{2}m_\varrho^2\vec{\varrho}_\mu(x)\vec{\varrho}^\mu(x) - \frac{1}{4}\vec{G}_{\mu\nu}(x)\vec{G}^{\mu\nu}(x) \tag{2.5}$$

and the free contribution of the electromagnetic field

$$\mathcal{L}_A^0(x) = -\frac{1}{4}A_{\mu\nu}(x)A^{\mu\nu}(x), \tag{2.6}$$

where the field tensors are given in the usual way:

$$F_{\mu\nu}(x) = \partial_\mu \omega_\nu(x) - \partial_\nu \omega_\mu(x), \tag{2.7}$$

$$A_{\mu\nu}(x) = \partial_\mu A_\nu(x) - \partial_\nu A_\mu(x), \tag{2.8}$$

$$\vec{G}_{\mu\nu}(x) = \partial_\mu \vec{\varrho}_\nu(x) - \partial_\nu \vec{\varrho}_\mu(x). \tag{2.9}$$

The interaction terms $\mathcal{L}_{MN}(x)$ are given by:

$$\mathcal{L}_{\sigma N}(x) = g_\sigma \bar{\psi}(x)\varphi(x)\psi(x), \tag{2.10}$$

$$\mathcal{L}_{\omega N}(x) = -g_\omega \bar{\psi}(x)\gamma^\mu \omega_\mu(x)\psi(x), \tag{2.11}$$

$$\mathcal{L}_{\varrho N}(x) = -g_\varrho \bar{\psi}(x)\gamma^\mu \vec{\tau} \cdot \vec{\varrho}_\mu(x)\psi(x), \tag{2.12}$$

$$\mathcal{L}_{AN}(x) = -e\bar{\psi}(x)\gamma^\mu \frac{1+\tau_3}{2} A_\mu(x)\psi(x). \tag{2.13}$$

The Thomas–Fermi expression for the energy density can be derived in a standard way from the Lagrangian. Expanding the nucleon field operators locally into plane waves, while the meson– and electromagnetic field operators are replaced by their ground–state expectation values, one gets in the static case:

$$\begin{aligned} e_{TF}(r) = & \frac{1}{2}\left[\left(\vec{\nabla}\varphi(r)\right)^2 + m_\sigma^2 \varphi^2(r)\right] - \\ & - \frac{1}{2}\left[\left(\vec{\nabla}\omega_0(r)\right)^2 + m_\omega^2 \omega_0^2(r)\right] - \\ & - \frac{1}{2}\left[\left(\vec{\nabla}\varrho_{00}(r)\right)^2 + m_\varrho^2 \varrho_{00}^2(r)\right] - \\ & - \frac{1}{2}\left(\vec{\nabla}A_0(r)\right)^2 + \\ & + g_\omega \omega_0(r)\rho_B(r) + g_\varrho \varrho_{00}(r)\rho_3(r) + eA_0(r)\rho_p(r) + \\ & + \sum_{i=p,n} \frac{1}{8\pi^2}\left[p_F(r)\varepsilon_F^3(r) + p_F^3(r)\varepsilon_F(r) - M^{*4}(r)\ \ln\frac{p_F(r)+\varepsilon_F(r)}{M^*(r)}\right]_i \end{aligned} \tag{2.14}$$

with the effective mass

$$M^*(r) = M - g_\sigma \varphi(r), \tag{2.15}$$

the densities

$$\rho_i(r) = \frac{1}{3\pi^2} p_{F_i}^3(r), \qquad i = p, n, \tag{2.16}$$

$$\rho_B(r) = \rho_p(r) + \rho_n(r), \tag{2.17}$$

$$\rho_3(r) = \rho_p(r) - \rho_n(r) \tag{2.18}$$

and

$$\varepsilon_{F_i}(r) = \sqrt{p_{F_i}^2(r) + M^{*2}(r)}, \qquad i = p, n. \tag{2.19}$$

$i = p, n$ denotes the charge state of each nucleon. The assumption of spherical symmetry leaves the time–like components of the vector meson fields, while only the uncharged component of the ϱ–meson contributes due to charge conservation. We neglect any contribution of antinucleons. In the following the indices of the ω–, ϱ– and electromagnetic field are dropped for simplicity.

The variational principle applied to equation (2.14) yields:

$$\left(\Delta - m_\sigma^2\right)\varphi(r) = -g_\sigma \rho_S(r), \tag{2.20}$$

$$\left(\Delta - m_\omega^2\right)\omega(r) = -g_\omega \rho_B(r), \tag{2.21}$$

$$\left(\Delta - m_\varrho^2\right)\varrho(r) = -g_\varrho \rho_3(r), \tag{2.22}$$

$$\Delta A(r) = -e\rho_p(r), \tag{2.23}$$

$$\mu_p = g_\omega \omega(r) + g_\varrho \varrho(r) + eA(r) + \varepsilon_{F_p}(r), \tag{2.24}$$

$$\mu_n = g_\omega \omega(r) - g_\varrho \varrho(r) + \varepsilon_{F_n}(r) \tag{2.25}$$

with the scalar densities

$$\rho_{S_i}(r) = \frac{2}{(2\pi)^3} \int_0^{p_{F_i}(r)} d^3p \, \frac{M^*(r)}{\sqrt{p^2 + M^{*2}(r)}}, \qquad i = p, n, \tag{2.26}$$

$$\rho_S(r) = \rho_{S_p}(r) + \rho_{S_n}(r). \tag{2.27}$$

Equations (2.20) to (2.27) constitute a nonlinear system for the nuclear densities, meson– and electromagnetic fields in RTFA, which has to be solved selfconsistently. At each iteration step the chemical potentials can be adjusted to the right number of protons and neutrons, Z and N, respectively, by

$$\int_V d^3r \, \rho_i(r) = \begin{cases} Z & \text{for } i = p \\ N & \text{for } i = n \end{cases}. \tag{2.28}$$

For the kinetic energy density one obtains in RTFA the following expression [16]:

$$\tau_{TF}(r) = \sum_{i=p,n} \left\{ \frac{1}{8\pi^2} \left[2p_F(r)\varepsilon_F^3(r) - M^{*2}(r) \left(5 - 4\frac{M}{M^*(r)} \right) p_F(r)\varepsilon_F(r) + \right.\right.$$

$$\left.\left. + M^{*4}(r) \left(3 - 4\frac{M}{M^*(r)} \right) \ln \frac{p_F(r) + \varepsilon_F(r)}{M^*(r)} \right] - M \frac{p_F^3(r)}{3\pi^2} \right\}_i . \qquad (2.29)$$

3 Quantum Corrections

In the general Hartree–Fock scheme the σ–meson gives the following contribution to the selfenergy in the phase–space representation:

$$\Sigma_\sigma(\vec{r}, p) = g_\sigma^2 \int_V d^3r' \, v^{(\sigma)} (\vec{r} - \vec{r}') \, \rho_S(\vec{r}') + \qquad (3.1)$$

$$+ \; i \, g_\sigma^2 \int \frac{d^4q}{(2\pi)^4} \frac{1}{(p-q)^2 - m_\sigma^2 + i\eta} G(\vec{r}, q) = \Sigma_\sigma^H(\vec{r}) + \Sigma_\sigma^F(\vec{r}, p).$$

The expressions for the other mesons have a similar structure [17]. $v^{(\sigma)}(\vec{r} - \vec{r}')$ represents the static meson propagator (Yukawa potential), while $G(\vec{r}, q)$ is the Wignertransform of Green's function, which obeys the corresponding Dyson equation. The Wignertransforms of the selfenergy and the Dyson equation constitute the relativistic Hartree–Fock approximation in phase–space, which is difficult to solve. For that reason we try an approximate solution by utilizing a $\hbar$–expansion. In the next section we discuss the Wigner–Kirkwood corrections, while section 3.2 deals with the Fock terms.

3.1 Wigner–Kirkwood Corrections

In Ref. [16] we derived the WK–corrections to the relativistic phase–space densities and densities up to second order in $\hbar$. The explicit expressions for the second order terms of the particle–, scalar–, energy– and kinetic energy densities of each kind of nucleons feeling the action of a scalar– and a time-like potential, Σ_S and Σ_0, respectively, are given in Appendix A.

Equations (2.16), (2.26), (2.14) and (2.29) represent the corresponding zeroth order expressions of the $\hbar$–expansion of Ref. [16], with the energy density e_{TF} depending on the definition of the interaction.

With the dynamics of the system specified by the Lagrangian (2.1), the scalar– and time–like parts of the nucleon selfenergy are given in each order by

$$\Sigma_S(r) = g_\sigma \varphi(r), \tag{3.1.1}$$

$$\Sigma_{0_p}(r) = g_\omega \omega(r) + g_\varrho \varrho(r) + eA(r), \tag{3.1.2}$$

$$\Sigma_{0_n}(r) = g_\omega \omega(r) - g_\varrho \varrho(r) \tag{3.1.3}$$

and the general expressions (A.5) and (A.6) are equivalent and equal to equations (2.24), (2.25) and (2.15), respectively. The $\hbar$–corrections to the meson– and electromagnetic fields are formally determined in each order by a set of equations analogue to the Thomas–Fermi equations (2.20) – (2.23) [17]. For the second order they are explicitly given in Appendix A.

Equations (2.14), (A.3) and (2.16), (A.1) constitute expressions up to second order in $\hbar$ for the energy– and particle density, respectively:

$$e = e_{TF} + \sum_{i=p,n} e_i^{WK}, \tag{3.1.4}$$

$$\rho_i = \frac{1}{3\pi^2} p_{F_i}^3 + \rho_i^{WK}, \qquad i = p, n. \tag{3.1.5}$$

At this point we remind the reader of the two crucial problems we mentioned in the Introduction, nameley the complicated functional dependence of expressions (3.1.4) and (3.1.5) on the meson– and the electromagnetic fields, their first and second derivatives and the Fermi momenta, and secondly the divergences of the WK–corrections (A.1) to (A.4) at the classical turning point.

As also mentioned in the Introduction both of the problems can be overcome by the density functional formalism [19, 21, 22] which, on the other hand, "loses information" with respect to the WK–approach. To study the impact of the "original" WK–corrections, while the simplicity and systematic structure of the semiclassical approach are retained, a kind of *perturbative* treatment seems necessary.

For this purpose we rewrite equation (2.28) as:

$$\int_V d^3r\, \rho_i(r) = \int_V d^3r \left[\frac{1}{3\pi^2} p_{F_i}^3(r) + \rho_i^{WK}(r)\right] = \begin{cases} Z = Z_{TF} + Z_{WK} & \text{for } i = p \\ N = N_{TF} + N_{WK} & \text{for } i = n \end{cases} \tag{3.1.6}$$

which takes terms of the order $\hbar^2$ into account. To consider the WK–corrections within our numerical iteration scheme we proceeded as follows: after a Thomas–Fermi run of our code (see section 2) we used its outcome to calculate the WK–corrections to the nucleon densities given by equation (A.1). Remembering the fact that only WK–corrections to expectation values of one body operators make sense, we integrate those expressions and obtain Z_{WK} and N_{WK} of (3.1.6). Before starting the next Thomas–Fermi iteration step, the chemical potentials have to be adjusted to the right particle numbers. But now, instead of adjusting them to Z and N as it is done within pure Thomas–Fermi calculations, we use $Z_{TF} = Z - Z_{WK}$ and $N_{TF} = N - N_{WK}$, respectively. This procedure is repeated until convergence is reached. In the final step of calculating the total energy, we include the WK–corrections to the energy density and to the meson– and electromagnetic fields, as determined by equations (A.3) and (A.8) – (A.11), respectively.

This iteration scheme provides a *perturbative* consideration of the WK–corrections to the particle numbers, while their given values Z and N are retained; i.e. comparisons with pure Thomas–Fermi calculations make sense, because one is really looking at the same nucleus. The perturbative character of the approach ensures that the consideration of the WK–corrections is restricted to order $\hbar^2$; i.e. only zeroth order quantities are used to calculate Z_{WK} and N_{WK}. In the following, we refer to this approximation scheme as RTFA–WK.

3.2 Exchange Corrections

Exchange terms are typical quantum corrections. This can be seen by looking at equation (3.1) in a system of units with $\hbar \neq 1$: the Fock terms are at least of the order $\hbar^2$ and hence of the same order as the WK–corrections of equations (A.1) to (A.4) [17]. Therefore, dealing with quantum corrections up to the second order, both kinds of corrections have to be taken into account.

Another motivation to include exchange corrections is the following: as is well known, in the original Walecka– (Hartree–) model, the incompressibility K of nuclear matter is considerably too large, while the nuclear matter effective mass M^*, which, for fixed saturation density and binding energy determines completely the energy dependence of the optical potential, is too small. A widely and successfully used (see, for instance, Refs. [4, 5, 9, 21, 22]) approach to overcome these shortcomings was firstly proposed by Boguta and

Bodmer [3], who introduced two additional free parameters through cubic and quartic terms in the scalar field, which shift K and M^* to more reasonable values compared with the experiment.

On the other hand, nuclear matter calculations within the Hartree–*Fock* scheme showed [6, 27] that to some extend these improvements can also be reached by inclusion of the π–meson and an additional tensor coupling term to the ϱ–nucleon interaction, but *without* "paying" for it by additional adjustable parameters.

Therefore and due to the arguments given in the Introduction in favour of more sophisticated many–body dynamics, we extend the Lagrangian to the standard Hartree–Fock form (see, for instance, Refs. [6, 17, 27, 28, 30]):

$$\mathcal{L}_2 = \mathcal{L}_1 + \mathcal{L}_\pi^0 + \mathcal{L}_{\pi N} + \mathcal{L}_{\varrho N}^{tensor}. \tag{3.2.1}$$

$\mathcal{L}_1$ denotes the original Lagrangian (2.1), while the free π–meson contribution is given by

$$\mathcal{L}_\pi^0(x) = \frac{1}{2}\left(\partial_\mu \vec{\pi}(x) \cdot \partial^\mu \vec{\pi}(x) - m_\pi^2\, \vec{\pi}(x) \cdot \vec{\pi}(x)\right). \tag{3.2.2}$$

For the π–nucleon interaction we use the pseudovector form [6]:

$$\mathcal{L}_{\pi N}(x) = -\frac{f_\pi}{m_\pi}\bar{\psi}(x)\gamma_5\gamma_\mu\left(\partial^\mu \vec{\tau} \cdot \vec{\pi}(x)\right)\psi(x), \tag{3.2.3}$$

while the tensor part of the ϱ–nucleon coupling can be written as:

$$\mathcal{L}_{\varrho N}^{tensor}(x) = -\frac{f_\varrho}{4M}\bar{\psi}(x)\sigma^{\mu\nu}\vec{\tau} \cdot \vec{G}_{\mu\nu}(x)\psi(x) \tag{3.2.4}$$

with

$$\sigma^{\mu\nu} = \frac{i}{2}\left[\gamma^\mu, \gamma^\nu\right]. \tag{3.2.5}$$

The tensor part of the ω–nucleon interaction is negligible [6].

The full selfconsistent treatment of the exchange corrections up to second order in $\hbar$ is a rather complicated task [17]. However, it has been shown in Ref. [28, 29] that within Hartree–Fock calculations for nuclear matter there are only small deviations when the Fock terms are determined perturbatively with the selfconsistently calculated Hartree results as an input, compared to the fully selfconsistent procedure. It is also known from nuclear

matter Hartree–Fock calculations that Σ_S^F and Σ_0^F, the scalar– and time–like components of the exchange part of the nucleon selfenergy, respectively, are reasonably independent of momentum and that the corresponding vector–like component Σ_V^F is a small correction ($< 5\%$) to the total nucleon selfenergy for the densities of interest in the present study (see, for instance, [6, 30]).

For these reasons we proceeded as follows: after a Thomas-Fermi iteration we used the resulting Fermi momenta and effective mass to calculate $\Sigma_S^F(r,p)$ and $\Sigma_0^F(r,p)$; i.e. the scalar– and time–like components of the exchange corrections within a *local density approximation* (LDA). To adjust the chemical potentials to the right particle numbers by (2.28), we rewrite equations (2.24) and (2.25) as:

$$\begin{aligned}\mu_p &= g_\omega\omega(r) + g_\varrho\varrho(r) + eA(r) + \Sigma_{0_p}^F(r) + \\ &\quad + \sqrt{p_{F_p}^2(r) + \left(M^*(r) - \Sigma_{S_p}^F(r)\right)^2}\,, \qquad (3.2.6)\\ \mu_n &= g_\omega\omega(r) - g_\varrho\varrho(r) + \Sigma_{0_n}^F(r) + \\ &\quad + \sqrt{p_{F_n}^2(r) + \left(M^*(r) - \Sigma_{S_n}^F(r)\right)^2}\,; \qquad (3.2.7)\end{aligned}$$

i.e. we treat the scalar– and time–like exchange terms, which are calculated within a LDA, like Thomas–Fermi contributions to the nucleon selfenergy. As it is done in Ref. [30], we take the Fock contributions at the corresponding Fermi momentum. Then the next Thomas–Fermi iteration starts until convergence is reached.

This iteration scheme considers the exchange corrections in a simple way, which allows a systematic study of their impact on the ground–state properties of a given nucleus with mass number A=Z+N. In the final step of calculating the total energy, the small corrections of Σ_V^F are also taken into account, calculated with the final Thomas–Fermi outcome in a pure perturbative manner.

Since the explicit expressions for Σ_S^F, Σ_0^F and Σ_V^F are rather lenghty and given in several publications concerning nuclear matter calculations (see, for instance, Refs. [1, 28, 31]), we will not repeat them and refer in this respect to the literature.

We denote the approach including the exchange corrections RTFA–EX, while the approximation scheme considering both quantum corrections up to the order $\hbar^2$, WK–corrections of section 3.1 and exchange corrections, is refered to as RTFA–QC.

4 Results And Discussion

In this section we present the results obtained within the different approximations described in sections 2 and 3. For the pure Thomas–Fermi (RTFA) calculations we used the set of parameters H1 [27], displayed in Table 1. The same parameters are used for RTFA–WK calculations. For the models with exchange corrections we have chosen the sets HF1 [27] and HF2 [32], which are also given in Table 1. The meson masses are fixed to their physical values $m_\omega = 783$ MeV, $m_\varrho = 770$ MeV and $m_\pi = 138$ MeV, while the bare nucleon mass is taken as $M = 939$ MeV. In order not to use too many free parameters, the ϱ–nucleon and, in the cases of HF1 and HF2, the tensor ϱ–nucleon and π–nucleon coupling constants were also fixed to their physical values, namely $g_\varrho^2/4\pi = 0.55$, $f_\varrho/g_\varrho = 6.6$ and $f_\pi^2/4\pi = 0.08$, known from scattering data [6]. The mass of the σ–meson is supposed to represent the exchange of a two π–resonance and should lie between 400 and 600 MeV. Within Hartree calculations for nuclear matter m_σ is not an adjustable parameter, because only the *ratios* of coupling constants to the corresponding meson–masses enter the expressions, but by inclusion of Fock terms, the meson–masses and hence m_σ occur seperatly.

Therefore, in the case of H1 there are only two adjustable parameters, the σ– and ω–nucleon coupling constants. Inclusion of exchange corrections (HF1 and HF2) adds the σ–meson mass as free parameter. g_σ and g_ω are chosen to reproduce the empirical saturation point of nuclear matter, $E/A =$ –15.75 MeV and $p_F^0 = 1.30$ fm^{-1} ($\rho^0 = 0.1484$ fm^{-3}). In HF1 we retain the value for m_σ from the H1 set (where it has no impact on the nuclear matter results). In HF2 m_σ is adjusted to get the experimental charge r.m.s. radius for ^{16}O within our RTFA–QC approach and turns out to be $m_\sigma = 497$ MeV.

As already mentioned earlier, pure Walecka– (Hartree–) calculations (H1) yield a nuclear matter incompressibility K, which is much too large, while, in view of the energy dependence of the optical potential, the effective mass M^* is too small. As shown in Table 1, the consideration of exchange terms shifts K and M^* to not yet perfect but more reasonable values compared with the experimental data. The adjustment of m_σ in HF2 affects the nuclear matter properties only slightly (the variation of K is smaller than 2.5%) but has significant influence on the results for finite systems, as we will see later.

4.1 Energies And Charge Radii

Before discussing the results for the energies and charge r.m.s radii within the different approaches presented in this paper, two remarks have to be made.

Firstly, to obtain expectation values of one body operators, like the particle numbers Z, N or the total and the kinetic energy E and T_{kin} within the approximations including WK–corrections (RTFA–WK, RTFA–QC), one has to evaluate the volume integrals of expressions (A.1), (A.3) and (A.4), respectively. As already mentioned in section 1, these expressions are distributions in the mathematical sense with divergences at the classical turning point. Due to this fact, it is not possible to determine r–space densities including WK–corrections to improve corresponding Thomas–Fermi predictions. This is a fundamental theoretical restriction of the approaches RTFA–WK and RTFA–QC. On the other hand the treatment of the divergences while evaluating volume integrals of WK–corrections is a purely technical and numerical problem. In the case of a given external potential, Krivine et.al. [20] showed a way to calculate these integrals analytically. This is not possible for a self-consistently determined potential and thus a numerical "solution" becomes necessary. Performimg volume integrals of WK–corrections, we used a cutoff at the classical turning point. A possible measure for the quality of this procedure is the reproduction of the particle numbers by equation (3.1.6). The maximum relative error we found is $\sim 0.6\%$ for the neutron number N of ^{16}O within the RTFA–QC approach. In all the other cases the relative errors for the particle numbers are smaller, for larger nuclei roughly by an order of magnitude. Hence, the results including WK–corrections can be considered as sufficiently reliable from the numerical point of view.

The second remark concerns center–of–mass corrections to the total energy, $E_{c.m.}$. It was explicitly shown for the nonrelativistic case in Ref. [33] that on a Thomas–Fermi level center–of–mass corrections to the total energy are absent. The inclusion of WK–corrections causes center–of–mass corrections. If one treats them in the standard manner, they are overestimated by $\sim 30 - 40\%$ for light and by a factor of $\sim 2 - 3$ for heavy nuclei [33]. Due to this reason we have neglected them in this study.

We turn now to the discussion of the total energies and charge r.m.s. radii calculated within the different approximations described in sections 2 and 3. For the characteristic set of spherical nuclei ^{16}O, ^{40}Ca, ^{90}Zr and ^{208}Pb the results are displayed in Table 2 along with the experimental values [6, 34–36].

RTFA–EX1, RTFA–QC1 and RTFA–EX2, RTFA–QC2 denote calculations with the set of parameters HF1 and HF2 of Table 1, respectively.

For all nuclei under consideration, the inclusion of WK–corrections (RTFA–WK) yields considerably stronger bound systems compared with the pure Thomas–Fermi calculations (RTFA). It is the nature of WK–corrections containing first and second derivatives of the potentials, to improve a Thomas–Fermi approach in the *surface region*, where the RTFA–assumption of locally constant meson fields becomes less and less valid. Thus the surface energy is a reasonable candidate when looking for the reason for the stronger binding within the RTFA–WK approach. A proper calculation of the surface energy demands the investigation of a semi–infinite system. In the present paper we restrict ourselves to a simple estimate. For this purpose we write the semiempirical mass formula as:

$$\frac{E}{A} = -a_V + a_S A^{-\frac{1}{3}}. \tag{4.1.1}$$

The volume energy coefficient a_V is given by the energy per nucleon of saturated nuclear matter, namely $a_V = 15.75$ MeV (see Table 1). a_S denotes the surface energy coefficient. We neglect the $A^{-\frac{2}{3}}$–term in the energy expansion (4.1.1), which is about one order of magnitude smaller than the surface energy. The functional form of the coefficients of the energy expansion up to the order $A^{-\frac{2}{3}}$ follows the droplet model theory of Myers and Swiatecki [37]. Coulomb– and asymmetry energy terms are also omitted in equation (4.1.1) and therefore we recalculated the symmetric systems ^{16}O and ^{40}Ca with the electromagnetic field switched off. Inserting the resulting energies into the l.h.s. of expression (4.1.1) we obtained a decrease of the surface energy coefficient from $a_S \sim 24.5$ MeV within RTFA calculations to $a_S \sim 19.5$ MeV for the RTFA–WK approach, while the experimental value of a_S for symmetric systems is around ~ 20 MeV. Though this procedure gives only a rough estimate of a_S, it allows a qualitative understanding of the stronger binding by inclusion of the WK–corrections due to a more realistic description of the surface energy.

Comparing RTFA calculations with the RTFA–EX1 approach, where exchange corrections are taken into account, a similar behaviour, namely a stronger binding for all nuclei under consideration, can be observed. Applying the same procedure as described above, we find a decrease of the surface energy coefficient from $a_S \sim 24.5$ MeV for the RTFA approach to

$a_S \sim 21$ MeV within RTFA–EX1 calculations. This can be understood in terms of the nuclear matter incompressibility K: inclusion of exchange corrections along with π–meson and tensor ϱ–nucleon contributions while the σ–meson mass m_σ remains fixed, causes a significant lower and more realistic value for K (see H1 and HF1 in Table 1). A lower incompressibility results in a smaller surface energy which in turn gives a stronger bound system.

Finally the RTFA–QC1 approach considers WK– and exchange–corrections. Now both effects, the smaller nuclear matter incompressibility and the improvement of the surface description by consideration of the spatial dependence of the meson fields, operate together resulting in a further decrease of the surface energy and stronger bindings compared to the RTFA–WK and RTFA–EX1 approaches, where WK– and exchange corrections have been considered separately, respectively.

Compared to the experimental values, pure Thomas–Fermi calculations (RTFA) give an underbinding for all nuclei under consideration. Due to the better description of the surface energy, inclusion of WK– or exchange corrections shifts the total energies E to more reasonable values (RTFA–WK, RTFA–EX1). Except for the case of ^{16}O, the RTFA–QC1 approach, which considers both quantum corrections, overestimates the binding compared to the experiment. This might be connected with the perturbative character of the approximations as described in section 3. Further improvement may be achieved by the consideration of $\hbar$–corrections of higher order.

Looking at the charge r.m.s. radii r_c one realizes that the inclusion of WK–corrections hardly affects their values (unsystematic variations of less than 0.5%) compared with pure Thomas–Fermi calculations. The situation is different, when exchange corrections are taken into account. Comparing the charge r.m.s. radii calculated within the RTFA–EX1 approach with the RTFA results, they are systematically smaller by about $1 \sim 2$ %, consistend with the larger binding energies provided by the inclusion of exchange corrections. A corresponding trend can be observed for the analogue "transition" from the RTFA–WK to the RTFA–QC1 approach, which also differ through the consideration of exchange corrections in the latter one. Compared to the experiments [34–36], all the values for r_c within the exchange corrected approaches RTFA–EX1 and RTFA–QC1 are too small.

As already mentioned earlier, the inclusion of Fock-terms into nuclear matter calculations introduces the σ–meson mass m_σ as a third adjustable parameter. We now want to study its impact on the properties of finite

systems in a systematic way. In the set of parameters HF2 of Table 1, m_σ is adjusted to get the experimental charge radius for ^{16}O within our RTFA–QC approach. The resulting decrease to $m_\sigma = 497$ MeV is not a surprise: the σ–meson contribution represents almost the entire attractive part of the nuclear potential, whose range is therefore determined by m_σ. Thus for a larger r_c, a smaller m_σ is necessary. As a consequence, for all nuclei under consideration the values for r_c increase within RTFA–EX2 and RTFA–QC2 calculations compared with the RTFA–EX1 and the RTFA–QC1 results, respectively, giving a better agreement with the experiments. In addition, the impact of m_σ weakens with increasing mass number A: for ^{16}O the variations of r_c between HF1– and HF2–calculations are about $\sim 3.5\,\%$, while for ^{208}Pb those differences go down to $\sim 0.04\,\%$. This is consistent with the fact that with increasing A the nuclear matter–like bulk region becomes more and more dominant and as we mentioned earlier, the impact of m_σ on nuclear matter properties is small (see Table 1).

Concerning the binding energies, the systems with larger r_c, calculated with the HF2–set, are less bound than the HF1–nuclei with their smaller charge r.m.s. radii. Estimating the surface energy coefficient as described above, the decrease of m_σ from 550 MeV to 497 MeV goes along with an increase of a_S by roughly $4 \sim 5$ MeV, which fixes it at about the same value as within pure RTFA calculations. Furthermore the nuclear matter incompressibility rises slightly by $2.3\,\%$ for the smaller m_σ (see Table 1). Thus, for the energy, the effects obtained by the inclusion of exchange corrections in comparison with RTFA are counteracted when m_σ is lowered. As for the charge r.m.s. radii, the same trend of a weakening influence of m_σ with increasing mass number A can be observed for the energies. The impact of m_σ on density distributions will be discussed in the following section.

To ascertain the importance of the WK–corrections to the energies, it is useful to look at the different contributions in some detail. In Table 3 we display the WK–corrections to the kinetic– (T_{kin}^{WK}/A) and potential (E_{pot}^{WK}/A) energies per nucleon along with the remaining contributions T_{kin}/A and E_{pot}/A within the approaches RTFA–WK and RTFA–QC1 for all nuclei under consideration. T_{kin}^{WK} represents the volume integral of expression (A.4), while E_{pot}^{WK} is the difference of the volume integral of equation (A.3) and T_{kin}^{WK}. We present the energies *per nucleon* to study their dependence on the mass number A. As one expects, the WK–corrections decrease with

increasing particle number. The values for T_{kin}^{WK}/A and E_{pot}^{WK}/A for ^{208}Pb are $40 \sim 60\,\%$ smaller than the corresponding ones for ^{16}O, due to the greater influence of the surface region in the latter case. A similar, though somewhat smaller trend can be observed for the WK–contributions within the RTFA–WK approach compared to those of RTFA–QC1 calculations: the values in the latter case are significantly smaller, because, as described above, the additionally considered exchange corrections (included in T_{kin}/A and E_{pot}/A) "help" the WK–corrections to improve the description of the surface. Finally, in all the cases the WK–corrections mainly "correct" the kinetic energies; their impact on the potential energies is clearly smaller.

The way the total energy is distributed among the various contributions is displayed in Tables 4 and 5 for all nuclei and all approaches under consideration. The upper index "ex" denotes exchange contributions, T_{kin} is, as in Table 3, the total kinetic energy without WK–corrections, while the total WK–corrections are included in E^{WK}. In all cases, the dominant contributions are the Thomas–Fermi terms of the σ– and ω–meson, E_σ and E_ω, respectively. The corresponding ϱ–meson contribution, E_ϱ, is negligible for symmetric nuclei, but has to be considered for ^{208}Pb.

While the nuclear saturation mechanism is almost entirely based on the remarkably balanced cancellation between E_σ and E_ω within the RTFA and RTFA–WK approaches, the situation is modified by the inclusion of exchange corrections. There is a contribution to the attractive part of the nuclear potential by the ω–exchange correction, E_ω^{ex}, of $\sim 10\,\%$, while the terms E_σ^{ex}, E_ϱ^{ex} and E_π^{ex} are repulsive, "supporting" E_ω. The π–meson, which appears only within the exchange corrected approaches, contributes $9 \sim 10\,\%$ to the repulsive part of the nuclear potential, while the ϱ–meson exchange corrections, E_ϱ^{ex}, are not negligible, independent on the proton–neutron asymmetry of the system. The total sum of each column adds up to the corresponding total energy in Table 2.

4.2 Densities And Spin–Orbit Interaction

We now turn to the discussion of various nuclear densities. In the previous sections we have characterized the WK–corrections as distributions in the mathematical sense. Therefore, plots of r–space densities within the RTFA–WK and RTFA–QC approaches display divergences at the classical turning point. However, we have the interesting possibility to study the impact of exchange corrections by comparing RTFA– with RTFA–EX calculations. We may obtain by this comparison essential hints about the role of exchange corrections in a simple manner. One further goal is to study the role of m_σ.

In Figs.1–4 we present the calculated charge density distributions ρ_c for all nuclei under consideration within the RTFA– and RTFA–EX1 approximations along with 3–parameter Fermi fits to the experimental data from Refs. [34–36]. The charge densities are calculated from the proton densities ρ_p (2.16) by:

$$\rho_c(r) = \int d^3r' \frac{1}{(r_0\sqrt{\pi})^3} \exp\left(-\left(\frac{(\vec{r}-\vec{r}')}{r_0}\right)^2\right) \rho_p(r') \tag{4.2.1}$$

with $r_0 = \sqrt{2/3}\ \langle r_p\rangle_{r.m.s.}$ and the charge r.m.s. radius of the proton taken as $\langle r_p\rangle_{r.m.s.} = 0.8$ fm [6]. Compared to the experiments, the calculated RTFA–densities are systematically too small in the bulk. Furthermore, the experimental surface behaviour (steepness) is not reproduced. Additionally, as expected, the quantal tails cannot be described correctly in a Thomas–Fermi treatment.

By inclusion of exchange corrections through the RTFA–EX1 approach, the bulk value of the charge density increases considerably in all cases; for ^{208}Pb it is in good agreement with the experiment. This corresponds to the higher binding energies for RTFA–EX1 nuclei, as discussed in the previous section (see Table 2). Furthermore, the smaller sizes provided by RTFA–EX1 calculations compared to RTFA are reflected in the density shapes: for ^{16}O inclusion of exchange terms reduces r_c by 1.1%. This relative reduction increases with A and is twice as large for ^{208}Pb (see Table 2). This A–dependent effect is clearly visible comparing the long–dashed and dot–dashed lines of Figs.1–4. Because the exchange terms are treated like Thomas–Fermi contributions to the nuclear potential; i.e. they are averaged in the same way (see section 3.2), one cannot expect any improvement in the quantal tails and,

of course, no shell–effects are obtainable in both treatments.

As mentioned in the previous section, changes in m_σ influence mainly small systems, while their impact is weakened for large, nuclear matter like nuclei. To study the m_σ–dependence of particle densities, we therefore look at the baryon densities ρ_B (see equation (2.17)) of the small systems ^{16}O and ^{40}Ca. This is done in Figs.5 and 6, where we have plotted the RTFA–, RTFA–EX1– and RTFA–EX2 results. As for the charge densities of Figs.1–4, the bulk values of ρ_B are higher within the RTFA–EX1 approximation compared to RTFA. The counteracting effect of a decreasing m_σ we discussed in the previous section and which leads to weaker bindings in RTFA–EX2 compared to RTFA–EX1 (see Table 2), yields in turn reduced corresponding bulk values of ρ_B. The diffuseness of the RTFA–EX2 densities are larger than the RTFA–EX1 ones. We observed similar trends for the charge densities, indicating that the higher values for the charge r.m.s. radii in RTFA–EX2 (see Table 2), are obtained by the longer tails of the charge densities rather than by an actual increase of the systems sizes. Confirming our previous statement concerning the dependence of the impact of m_σ on the mass number A, the differences between the RTFA–EX1– and RTFA–EX2 baryon densities are smaller for ^{40}Ca than for ^{16}O. We found that for ^{90}Zr and ^{208}Pb this trend continues.

We now turn to the discussion of kinetic energy densities. In Fig.7 we present the proton kinetic energy densities τ_p for our set of spherical nuclei within the RTFA (solid lines), RTFA–EX1 (long–dashed) and RTFA–EX2 (dot–dashed) approximations. As for the charge– and baryon densities of Figs.1–6, the values in the bulk are considerably higher when exchange terms are included. Comparing the RTFA–EX1 with the RTFA–EX2 results, the impact of m_σ in the bulk region is not as systematic as discussed above. However, similar to Figs.5 and 6, a more diffuse fall–off can be observed for the RTFA–EX2 interaction compared to RTFA–EX1. The peaks in the surface regions, even for the small nuclei where no central depression caused by the electromagnetic field occurs, reflect the dependence of the kinetic energy density on the effective mass (see equation (2.29) for RTFA), which approaches the bare nucleon mass at large radial distances.

At all radial distances τ_p is positive. This is what one expects for the semiclassical RTFA–model as well as for the RTFA–EX approaches, where exchange terms are treated like Thomas–Fermi contributions to the nuclear potential (see section 3.2). These approximations are principally not able to describe the physics of the classically forbidden region, where the quantal

tails of the particles' wave functions have negative kinetic energies, resulting in a negative kinetic energy density in the outer surface region. However, improvement of this deficiency of standard Thomas–Fermi methods is one of the reasons for the consideration of WK–corrections. Hence, we plotted in Fig.8 the Thomas–Fermi contribution τ_p^{TF} (see equation (2.29)) and the total proton kinetic energy density $\tau_p = \tau_p^{TF} + \tau_p^{WK}$ of ^{208}Pb within our RTFA–WK approach (τ_p^{WK} is given by equation (A.4)). Of course, this is "illegitimate" in view of the WK–corrections being distributions in the mathematical sense (see section 3.1), and the question concerning the physical nature of such a plot, and especially of the divergences, finally remains open to us (in this context see also Ref. [38]). However, considering the fact that the volume integral of τ_p is a reasonable physical quantity, it might be of interest that, while τ_p^{TF} stays positive at all radial distances as expected, the inclusion of WK–corrections yields a negative kinetic energy density in the surface region before it diverges at the classical turning point. Refering to the vague "loss of information" along with the reordering of the $\hbar$–expansion when going from the WK–approach to the density functional formalism (see section 1), this negative kinetic energy density might be a candidate: looking at Fig.5 of Ref. [21], the density functional formalism seems not to be able to provide negative values for τ_p at large radial distances (in a recent paper, Swiatecki [39] studied an improved nonrelativistic Thomas–Fermi method, in which the standard expression for the kinetic energy density is modified so that it becomes negative in the outer surface region).

Finally we turn to the discussion of the *spin–orbit interaction*. It is automatically included in the single–particle Dirac equation and can be identified by means of a Foldy–Wouthuysen reduction. For a nucleon feeling the action of a scalar– and a time–like potential, Σ_S and Σ_0, respectively, one obtains an effective single–particle spin–orbit interaction of the form [1, 40]:

$$V_{s.o.}(r) = \frac{1}{2M^2 r}\left(\frac{d\Sigma_0(r)}{dr} + \frac{d\Sigma_S(r)}{dr}\right)\mathbf{S}\cdot\mathbf{L} \equiv -\alpha(r)\,\mathbf{S}\cdot\mathbf{L}. \qquad (4.2.2)$$

We calculated the quantity α for a proton in all nuclei under consideration. Within the RTFA approximation, Σ_S and Σ_0 are given by equations (3.1.1) and (3.1.2), respectively. For RTFA–EX calculations we used in accordance with equation (3.2.6):

$$\Sigma_S(r) \;=\; g_\sigma\varphi(r) + \Sigma_{S_p}^F(r)\,, \qquad (4.2.3)$$

$$\Sigma_0(r) \;=\; g_\omega\omega(r) + g_\varrho\varrho(r) + eA(r) + \Sigma^F_{0_p}(r)\,, \qquad (4.2.4)$$

with the Fock contributions evaluated at the corresponding Fermi momentum. The results are presented in Fig.9. While Σ_S and Σ_0 are adding up in the spin–orbit interaction of equation (4.2.2), we know that they tend to cancel in the binding energy. Therefore we also plotted the differences of the scalar– and time–like components of the RTFA–proton–selfenergies, $\Sigma_S - \Sigma_0$, in Fig.9. These differences become negative for large radial distances because of the long–range Coulomb field, which is included in Σ_0.

The interesting parts are the peaks of α in the surface regions. It can be observed that the inclusion of exchange–corrections (RTFA– compared with RTFA–EX1 results) reduces the maximum value of α by roughly 9–12 %, while the lower m_σ (RTFA–EX1 compared with RTFA–EX2) causes an additional decrease of α_{max} of about the same magnitude. This latter effect is consistent with the larger diffuseness of RTFA–EX2 densities we discussed above.

Furthermore, α_{max} depends strongly on the mass number A. Within the RTFA approximation we found $\alpha_{max} = 3.08$ MeV for ^{16}O, but $\alpha_{max} = 1.19$ MeV for ^{208}Pb. This is clear in view of the larger radial distances involved for larger systems (see expression (4.2.2)) and means in turn that the strength of the spin–orbit splitting decreases with increasing orbital angular momentum. This trend agrees with experimental data (see Ref. [41]). Finally we compare our results for α_{max} in ^{40}Ca with the experimental value of the spin–orbit splitting for the odd proton in ^{41}Sc: within RTFA–, RTFA–EX1 and RTFA–EX2 calculations we obtained $\alpha_{max} = 2.19, 1.99$ and 1.78 MeV, respectively, while the experiment yields $\alpha = 1.80$ MeV [10]. Hence, our exchange corrected model is in rather close agreement with the empirical data.

5 Concluding Remarks

In the present paper we have carried out relativistic Thomas–Fermi calculations including quantum corrections for a set of spherical nuclei. There are two kinds of quantum corrections up to the second order in $\hbar$, which we incorporated perturbatively in our code, while the numbers of protons and neutrons are held fixed. First the WK–corrections, which are supposed to improve the expectation values of one body operators compared with pure Thomas–Fermi calculations. In this case we used a linear σ–ω model which reproduces the nuclear matter saturation point but yields a considerably too large nuclear matter incompressibility. The latter point causes a surface energy, which is too high within Thomas–Fermi calculations. Inclusion of WK–corrections significantly reduces the difference between the RTFA– and experimental value of the surface energy coefficient resulting in more realistic binding energies. This improvement within the RTFA–WK approximation is achieved by a better description of the nuclear surface through the consideration of the spatial dependence of the meson– and the electromagnetic fields and the possibility of a negative kinetic energy density in the surface region which characterizes the physics of the classical forbidden region. The impact of the WK–corrections decreases with increasing mass number.

The second kind of quantum corrections of the order $\hbar^2$ are exchange corrections. Here we also considered π–meson and tensor ϱ–nucleon contributions. This shifts the nuclear matter incompressibility to more reasonable values. In turn, we found the nuclear surface energy lowered by the exchange corrections by $\sim$ 14%, which yields stronger bindings and smaller charge r.m.s. radii compared with the RTFA approach. As a consequence, the bulk values of the charge–, particle– and kinetic energy densities are systematically higher within RTFA–EX calculations.

Within nuclear matter Hartree–Fock calculations, m_σ constitutes an adjustable parameter. We calculated a set of parameters with m_σ adjusted to get the experimental charge r.m.s. radius of ^{16}O and studied its influence on properties of nuclear matter and finite nuclei. While m_σ affects nuclear matter properties only slightly, it has significant influence on those of finite systems. With the σ–meson contribution representing almost the entire attractive part of the nuclear potential, m_σ determines its range. Hence we found that a lower m_σ yields larger r.m.s. radii, weaker bindings and lower bulk values of the various densities. The larger r.m.s. radii go along with a

more diffuse fall–off in the surface regions of the densities we investigated. The impact of m_σ weakens with increasing mass number according to the nuclear matter limit, where its influence is small.

Finally we calculated the spin–orbit interaction. We found that its strength decreases with both, the inclusion of exchange corrections and decreasing m_σ. In agreement with experimental data a strong dependence of the spin–orbit splitting on the mass number can be observed, namely smaller values with increasing A. The maximum value of the spin–orbit splitting we found within RTFA–EX calculations for a proton in ^{40}Ca is in good agreement with the experiment.

In summary, by including quantum corrections in the described approximate manner, our approach constitutes a simple and transparent model to study their impact on the properties of finite systems in a systematic way for nontrivial Lagrangians along with a tractable numerical effort in comparison with lengthy wavefunction calculations.

A Appendix

In this Appendix we give the explicit expressions for the second order WK–corrections to the particle–, scalar–, energy– and kinetic energy densities of *each kind of nucleons* feeling the action of a scalar– and a time–like potential, Σ_S and Σ_0, respectively (see Ref. [16]):

$$\begin{aligned}
\rho^{WK}(r) &= \frac{1}{24\pi^2}\Bigg[\frac{1}{p_F}\left(3-x_F^2\right)\left(\vec{\nabla}\Sigma_0\right)^2 - \\
&- \left(2x_F + 4\ln\frac{p_F+\varepsilon_F}{M^*}\right)\Delta\Sigma_0 + \\
&+ 2\frac{x_F}{M^*}\left(3-x_F^2\right)\vec{\nabla}\Sigma_0\cdot\vec{\nabla}M^* + \\
&+ \frac{1}{p_F}\left(2-x_F^2\right)\left(\vec{\nabla}M^*\right)^2 + \\
&+ 2\frac{p_F}{M^*}\left(1-x_F^2\right)\Delta M^*\Bigg],
\end{aligned} \tag{A.1}$$

$$
\begin{aligned}
\rho_S^{WK}(r) &= -\frac{1}{24\pi^2}\Bigg[\frac{x_F}{M^*}\left(1+x_F^2\right)\left(\vec{\nabla}\Sigma_0\right)^2 + \\
&+ 2\frac{M^*}{p_F}\Delta\Sigma_0 + \\
&+ \frac{2}{p_F}\left(2+x_F^2\right)\vec{\nabla}\Sigma_0\cdot\vec{\nabla}M^* + \\
&+ \frac{x_F}{M^*}\left(2+x_F^2\right)\left(\vec{\nabla}M^*\right)^2 + \\
&+ \left(2x_F - 6\ln\frac{p_F+\varepsilon_F}{M^*}\right)\Delta M^*\Bigg],
\end{aligned}
\tag{A.2}
$$

$$
\begin{aligned}
e^{WK}(r) &= \frac{1}{24\pi^2}\Bigg[\left(x_F\left(2-x_F^2\right) - 2\ln\frac{p_F+\varepsilon_F}{M^*}\right)\left(\vec{\nabla}\Sigma_0\right)^2 - \\
&- 2p_F\left(1+x_F^2\right)\Delta\Sigma_0 + \\
&+ 2\frac{M^*}{p_F}\left(1-x_F^2\right)\vec{\nabla}\Sigma_0\cdot\vec{\nabla}M^* + \\
&+ \left(x_F\left(1-x_F^2\right) - \ln\frac{p_F+\varepsilon_F}{M^*}\right)\left(\vec{\nabla}M^*\right)^2 - \\
&- 2M^*\left(x_F - \ln\frac{p_F+\varepsilon_F}{M^*}\right)\Delta M^*\Bigg] + \\
&+ \left(1-\frac{\lambda}{2}\right)\Sigma_0\,\rho^{WK}(r) + \frac{\lambda}{2}\Sigma_S\,\rho_S^{WK}(r)\ ,
\end{aligned}
\tag{A.3}
$$

$$
\begin{aligned}
\tau^{WK}(r) &= \frac{1}{24\pi^2}\Bigg[\left(\left(3-\left(1+x_F^2\right)\frac{M}{M^*}\right)x_F - \left(3-x_F^2\right)\frac{M}{p_F} - 2\ln\frac{p_F+\varepsilon_F}{M^*}\right)\left(\vec{\nabla}\Sigma_0\right)^2 + \\
&+ 2M\left(x_F - \frac{p_F}{M}\left(2-\left(1-x_F^2\right)\frac{M}{M^*}\right) + 2\ln\frac{p_F+\varepsilon_F}{M^*}\right)\Delta\Sigma_0 - \\
&- \left(\frac{2M}{p_F}\left(2+x_F^2\right) + 2x_F\frac{M}{M^*}\left(3-x_F^2\right) + 6\frac{p_F}{M^*}\left(1-x_F^2\right)\right)\vec{\nabla}\Sigma_0\cdot\vec{\nabla}M^* - \\
&- \left(\frac{M}{p_F}\left(2-x_F^2\right) - \left(3-2\frac{M}{M^*}\right)x_F + \frac{M}{M^*}x_F^3 + \ln\frac{p_F+\varepsilon_F}{M^*}\right)\left(\vec{\nabla}M^*\right)^2 - \\
&- 2M\left(x_F + \frac{p_F}{M^*}\left(1-x_F^2\right) - \left(3-2\frac{M^*}{M}\right)\ln\frac{p_F+\varepsilon_F}{M^*}\right)\Delta M^*\Bigg]
\end{aligned}
\tag{A.4}
$$

with ε_F given by (2.19) and the definitions:

$$p_F(r) := \sqrt{(\mu - \Sigma_0(r))^2 - M^{*2}(r)}, \tag{A.5}$$
$$M^*(r) := M - \Sigma_S(r) \tag{A.6}$$

and

$$x_F(r) := \frac{\varepsilon_F(r)}{p_F(r)}. \tag{A.7}$$

In equation (A.3) $\lambda = 0$ corresponds to a purely external potential, while $\lambda = 1$ describes the case of a selfconsistent two particle interaction.

For the Lagrangian (2.1) the decomposition of Σ_S and Σ_0 is given in each order of $\hbar$ by equations (3.1.1) - (3.1.3). The second order corrections to the meson– and electromagnetic fields are determined by [17]:

$$\left(\Delta - m_\sigma^2\right)\varphi^{WK}(r) = -g_\sigma\left(\rho_{S_p}^{WK}(r) + \rho_{S_n}^{WK}(r)\right), \tag{A.8}$$
$$\left(\Delta - m_\omega^2\right)\omega^{WK}(r) = -g_\omega\left(\rho_p^{WK}(r) + \rho_n^{WK}(r)\right), \tag{A.9}$$
$$\left(\Delta - m_\varrho^2\right)\varrho^{WK}(r) = -g_\varrho\left(\rho_p^{WK}(r) - \rho_n^{WK}(r)\right), \tag{A.10}$$
$$\Delta A^{WK}(r) = -e\rho_p^{WK}(r). \tag{A.11}$$

Acknowledgements

One of us, D. Von-Eiff, would like to thank the Deutscher Akademischer Austauschdienst for a scholarship and to express his gratitude to the Nuclear Theory Group at the LBL for the kind hospitality. Useful discussions with W.D. Myers, W.J. Swiatecki, F. Weber, W. Stocker and M. Centelles and the contribution that J. Ramschütz made by determining the set of parameters HF2 are gratefully acknowledged.

References

[1] B.D. Serot and J.D. Walecka, in "Advances in Nuclear Physics", Vol.16, ed. J.W. Negele and E. Vogt, Plenum Press, New York, London 1986; and references therein

[2] L.S. Celenza and C.M. Shakin, in "Lecture Notes in Physics", Vol.2, "Relativistic Nuclear Physics", World Scientific, Singapore 1986; and references therein

[3] J. Boguta and A.R. Bodmer, *Nucl. Phys.* **A292** (1977) 413

[4] Y.K. Gambhir, P. Ring and A. Thimet, *Ann. Phys. (N.Y.)* **198** (1990) 132

[5] P.-G. Reinhard et.al., *Z. Phys.* **A323** (1986) 13

[6] A. Bouyssy et.al., *Phys. Rev.* **C36** (1987) 380

[7] B. ter Haar and R. Malfliet, *Phys. Rep.* **149** (1987) 207

[8] H. Müther, R. Machleidt and R. Brockmann, *Phys. Lett.* **B202** (1988) 483; *Phys. Rev.* **C42** (1990) 1981

[9] J. Boguta and J. Rafelski, *Phys. Lett.* **B71** (1977) 22

[10] F.E. Serr and J.D. Walecka, *Phys. Lett.* **B79** (1978) 10

[11] B.D. Serot and J.D. Walecka, *Phys. Lett.* **B87** (1979) 172

[12] P. Ring and P. Schuck, "The Nuclear Many–Body Problem", Springer, Berlin 1980

[13] B. Grammaticos and A. Voros, *Ann. Phys. (N.Y.)* **123** (1979) 359; *Ann. Phys. (N.Y.)* **129** (1980) 153

[14] E. Wigner, *Phys. Rev.* **40** (1932) 749

[15] D. Von-Eiff and M.K. Weigel, *Z. Phys.* **A339** (1991) 63

[16] D. Von-Eiff, S. Haddad and M.K. Weigel, LBL–Preprint 31614, *Phys. Rev.* **C** (1992), in print

[17] M.K. Weigel, S. Haddad and F. Weber, *J. of. Phys.* **G17** (1991) 619

[18] M. Centelles et.al., *Nucl. Phys.* **A519** (1990) 73c

[19] C. Speicher, R.M. Dreizler and E. Engel, *Ann. Phys.* **213** (1992) 312

[20] H. Krivine, M. Casas and J. Martorell, *Ann. Phys.* **200** (1990) 304

[21] M. Centelles et.al., *Nucl. Phys.* **A537** (1992) 486

[22] M. Centelles et.al., "A Semiclassical Approach To Relativistic Mean Field Theory", Preprint, University of Barcelona 1992

[23] V.M. Strutinsky, *Nucl. Phys.* **A95** (1967) 420; *Nucl. Phys.* **A122** (1968) 1

[24] M. Centelles et.al., *Nucl. Phys.* **A510** (1990) 397

[25] Hsiao–bai Ai et.al., *Phys. Rev.* **C39** (1989) 236

[26] S. Marcos et.al., *Phys. Rev.* **C39** (1989) 1134

[27] M. Jetter, F. Weber and M.K. Weigel, *Europhys. Lett.* **14** (1991) 633

[28] F. Weber and M.K. Weigel, *Z. Phys.* **A330** (1988) 249

[29] A. Bouyssy et.al., *Phys. Rev. Lett.* **55** (1985) 1731

[30] C.J. Horowitz and B.D. Serot, *Nucl. Phys.* **A464** (1987) 613

[31] F. Weber and M.K. Weigel, *Nucl. Phys.* **A493** (1989) 549

[32] J. Ramschütz, private communication

[33] M. Brack, C. Guet and H.–B. Håkansson, *Phys. Rep.* **123** (1985) 275

[34] H. de Vries, C.W. de Jager and C. de Vries, *At. Data Nucl. Data Tables* **36** (1987) 495

[35] P.X. Ho et.al., *Nucl. Phys.* **A179** (1972) 529

[36] J. Heisenberg et.al., *Phys. Rev. Lett.* **23** (1969) 1402

[37] W.D. Myers and W.J. Swiatecki, *Ann. Phys. (N.Y.)* **55** (1969) 395

[38] M. Durand, P. Schuck and X. Viñas, "On The Curvature Energy Of Finite Fermi Systems", Preprint, Institut des Sciences Nucléaires de Grenoble 1991

[39] W.J. Swiatecki, LBL–Preprint 31582, *Nucl. Phys.* **A** (1992), in print

[40] W.A. Barker and Z.V. Chraplyvy, *Phys. Rev.* **89** (1953) 446

[41] J.M. Eisenberg and W. Greiner, in "Nuclear Theory", Vol.1, "Nuclear Models", North–Holland and American Elsevier, Amsterdam, Oxford, New York 1975, p.196

Table captions

table 1: Parameters and nuclear matter properties (energy per particle E/A, Fermi momentum p_F^0, incompressibility K and effective mass M^*/M at saturation) of the three forces considered in the text. Fixed input parameters are: $M = 939$ MeV, $m_\omega = 783$ MeV, $m_\varrho = 770$ MeV, $m_\pi = 138$ MeV; $g_\varrho^2/4\pi = 0.55$, $f_\varrho/g_\varrho = 6.6$ and $f_\pi^2/4\pi = 0.08$. $C_i^2 = g_i^2\ (M/m_i)^2\ , i = \sigma,\omega$.

table 2: Total energies (in MeV) and charge r.m.s. radii (in fm) of ^{16}O, ^{40}Ca, ^{90}Zr and ^{208}Pb calculated with the different approaches studied in this paper in comparison with the experimental values [6, 34–36].

table 3: Contributions of the WK–corrections to the kinetic (T_{kin}^{WK}/A) and potential (E_{pot}^{WK}/A) energies per nucleon of ^{16}O, ^{40}Ca, ^{90}Zr and ^{208}Pb within the two approximations RTFA–WK and RTFA–QC1. T_{kin}/A and E_{pot}/A denote the remaining contributions to the total kinetic and potential energies per nucleon. All quantities are in MeV.

table 4: Analysis of the total energies of ^{16}O and ^{40}Ca within the different approximations studied in this paper: T_{kin} and E_{Coul} denote the kinetic and Coulomb energies, respectively. E_σ, E_ω and E_ϱ are the Thomas–Fermi contributions to the potential energies coming from the exchange of σ–, ω– and ϱ–mesons, respectively. E_i^{ex}, $i = \sigma,\omega,\varrho,\pi,Coul$ denote the corresponding exchange corrections (Fock terms), while E^{WK} is the total WK–correction to the energies. The sum of the terms in each column gives the corresponding total energy listed in Table 2. All quantities are in MeV.

table 5: Same as Table 4 for ^{90}Zr and ^{208}Pb.

Table 1

	H1	HF1	HF2
m_σ (MeV)	550	550	497
C_σ^2	357.740	288.106	289.474
C_ω^2	274.105	146.656	150.372
E/A (MeV)	-15.75	-15.75	-15.75
p_F^0 (fm^{-1})	1.30	1.30	1.30
K (MeV)	545	394	403
M^*/M	0.541	0.599	0.594

Table 2

	^{16}O		^{40}Ca		^{90}Zr		^{208}Pb	
	E	r_c	E	r_c	E	r_c	E	r_c
RTFA	-80.85	2.68	-260.28	3.42	-645.98	4.27	-1412.03	5.52
RTFA–WK	-105.51	2.67	-317.36	3.43	-747.85	4.27	-1589.56	5.55
RTFA–EX1	-100.48	2.65	-315.05	3.36	-771.80	4.19	-1671.97	5.40
RTFA–EX2	-79.87	2.75	-273.43	3.43	-703.01	4.24	-1569.36	5.42
RTFA–QC1	-115.12	2.64	-367.04	3.36	-877.90	4.17	-1841.26	5.38
RTFA–QC2	-85.82	2.73	-308.08	3.43	-780.44	4.22	-1711.61	5.40
Exp.	-127.68	2.73	-342.00	3.48	-783.90	4.27	-1636.96	5.42

Table 3

RTFA–WK	^{16}O	^{40}Ca	^{90}Zr	^{208}Pb
T_{kin}/A	10.463	9.888	9.860	10.203
T_{kin}^{WK}/A	3.624	3.072	2.443	1.446
E_{pot}/A	-18.050	-18.663	-18.896	-18.133
E_{pot}^{WK}/A	-2.631	-2.232	-1.716	-1.158
RTFA–QC1				
T_{kin}/A	11.656	11.189	10.984	11.214
T_{kin}^{WK}/A	1.930	1.537	1.217	0.814
E_{pot}/A	-19.291	-20.500	-20.802	-19.990
E_{pot}^{WK}/A	-1.489	-1.401	-1.153	-0.890

Table 4

	^{16}O				^{40}Ca			
	RTFA	RTFA–WK	RTFA–EX1	RTFA–QC1	RTFA	RTFA–WK	RTFA–EX1	RTFA–QC1
T_{kin}	180.84	167.40	187.82	186.49	438.32	395.52	462.63	447.55
E_σ	–2001.68	–2058.49	–1662.15	–1711.60	–5786.36	–5834.05	–4903.21	–4969.13
E_ω	1723.21	1752.20	945.29	963.35	5007.02	5009.59	2803.80	2821.37
E_ϱ	0.01	0.02	0.00	0.01	0.06	0.15	0.03	0.06
E_{Coul}	16.88	16.71	17.07	17.21	80.94	78.04	82.48	81.51
E_σ^{ex}	–	–	386.86	395.78	–	–	1109.13	1113.35
E_ω^{ex}	–	–	–190.82	–194.73	–	–	–536.23	–536.90
E_ϱ^{ex}	–	–	67.78	69.96	–	–	228.95	230.90
E_π^{ex}	–	–	149.75	153.24	–	–	442.50	443.89
E_{Coul}^{ex}	–	–	–1.95	–1.96	–	–	–5.05	–4.97
E^{WK}	–	15.89	–	7.05	–	33.63	–	5.42

Table 5

	^{90}Zr				^{208}Pb			
	RTFA	RTFA–WK	RTFA–EX1	RTFA–QC1	RTFA	RTFA–WK	RTFA–EX1	RTFA–QC1
T_{kin}	964.20	887.36	1022.46	988.54	2256.92	2122.18	2398.65	2332.52
E_σ	–14070.55	–14157.92	–11993.47	–12086.91	–33876.49	–33610.76	–28926.76	–28965.15
E_ω	12200.23	12202.39	6870.59	6887.64	29342.46	28996.24	16545.90	16519.32
E_ϱ	4.58	5.30	4.66	4.67	40.67	43.16	42.09	39.67
E_{Coul}	255.80	249.94	261.32	261.49	824.65	799.31	843.49	851.58
E_σ^{ex}	–	–	2688.08	2683.34	–	–	6545.70	6503.92
E_ω^{ex}	–	–	–1284.52	–1279.74	–	–	–3111.80	–3088.02
E_ϱ^{ex}	–	–	592.53	593.23	–	–	1447.94	1446.51
E_π^{ex}	–	–	1076.59	1074.19	–	–	2563.23	2555.20
E_{Coul}^{ex}	–	–	–10.08	–10.06	–	–	–20.51	–20.69
E^{WK}	–	65.45	–	5.74	–	59.88	–	–15.77

Figure captions

figure 1: Charge density distribution for ^{16}O: Calculated folded values of ρ_c (Eq.(4.2.1)) within RTFA and RTFA–EX1 are compared with a 3–parameter Fermi fit to the experimental data [34].

figure 2: Same as Fig.1 for ^{40}Ca.

figure 3: Same as Fig.1 for ^{90}Zr. The experimental values are taken from [35].

figure 4: Same as Fig.1 for ^{208}Pb. The experimental values are taken from [36].

figure 5: Baryon density for ^{16}O: Calculated point (unfolded) values of ρ_B (Eq.(2.17)) within the RTFA–, RTFA–EX1– and RTFA–EX2–approaches.

figure 6: Same as Fig.5 for ^{40}Ca.

figure 7: Proton kinetic energy densities for all nuclei under consideration obtained in the RTFA (solid lines), RTFA–EX1 (long–dashed) and RTFA–EX2 (dot–dashed) approximations.

figure 8: RTFA contribution (solid line) and total (long–dashed) proton kinetic energy "density" of ^{208}Pb within the RTFA–WK approach.

figure 9: Radial distribution of the quantity $\alpha(r) \times 10$ for a proton in all nuclei under consideration obtained in the RTFA (dotted lines), RTFA–EX1 (long–dashed) and RTFA–EX2 (dot–dashed) approximations along with the difference of the scalar– and time–like components $(\Sigma_S - \Sigma_0)$ of the RTFA–proton–selfenergy (solid lines).

Fig.1

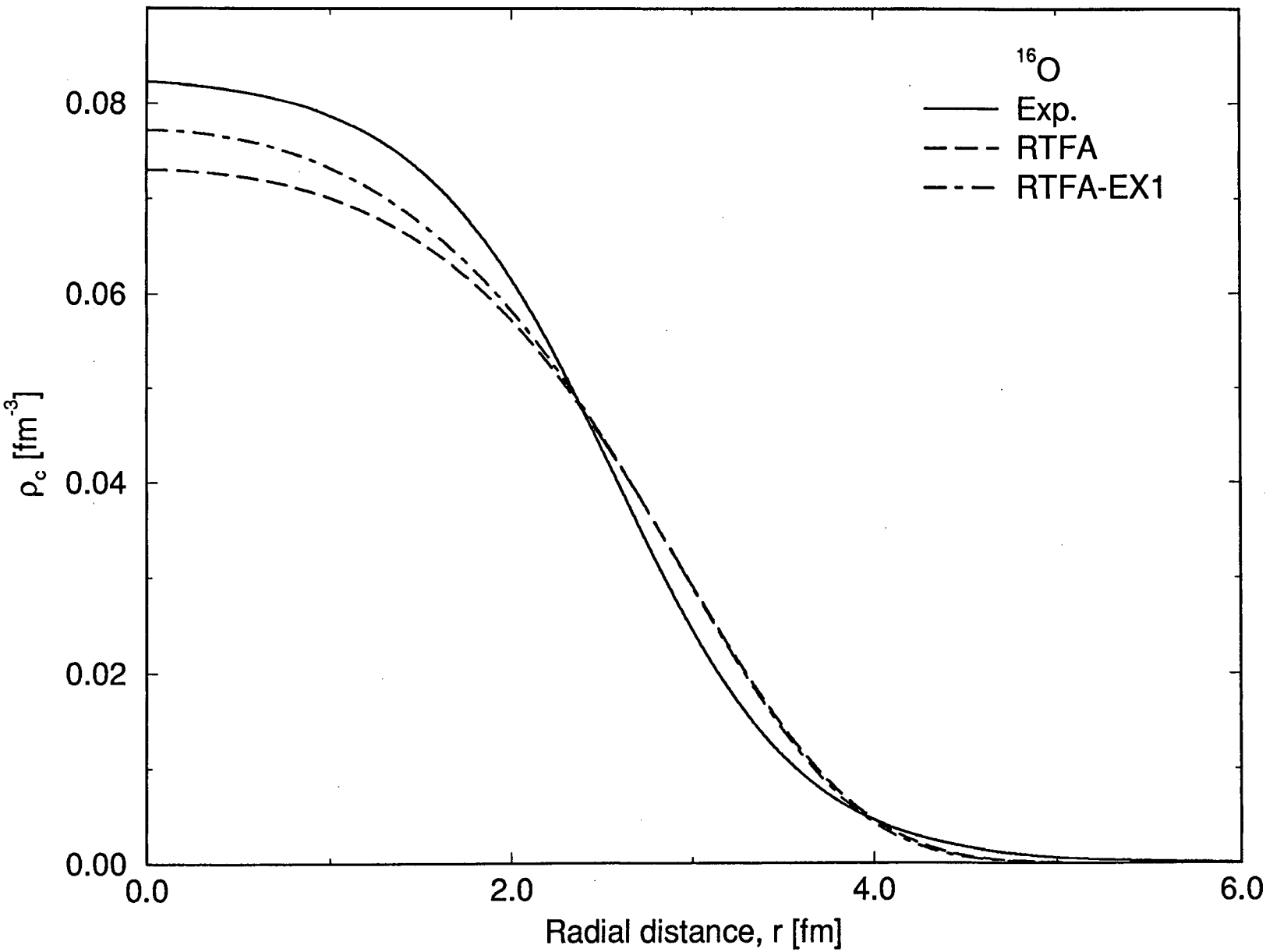
^{16}O
Exp.
RTFA
RTFA-EX1
0.08
0.06
0.04
0.02
0.00
ρ_c [fm^{-3}]
0.0
2.0
4.0
6.0
Radial distance, r [fm]

Fig.2

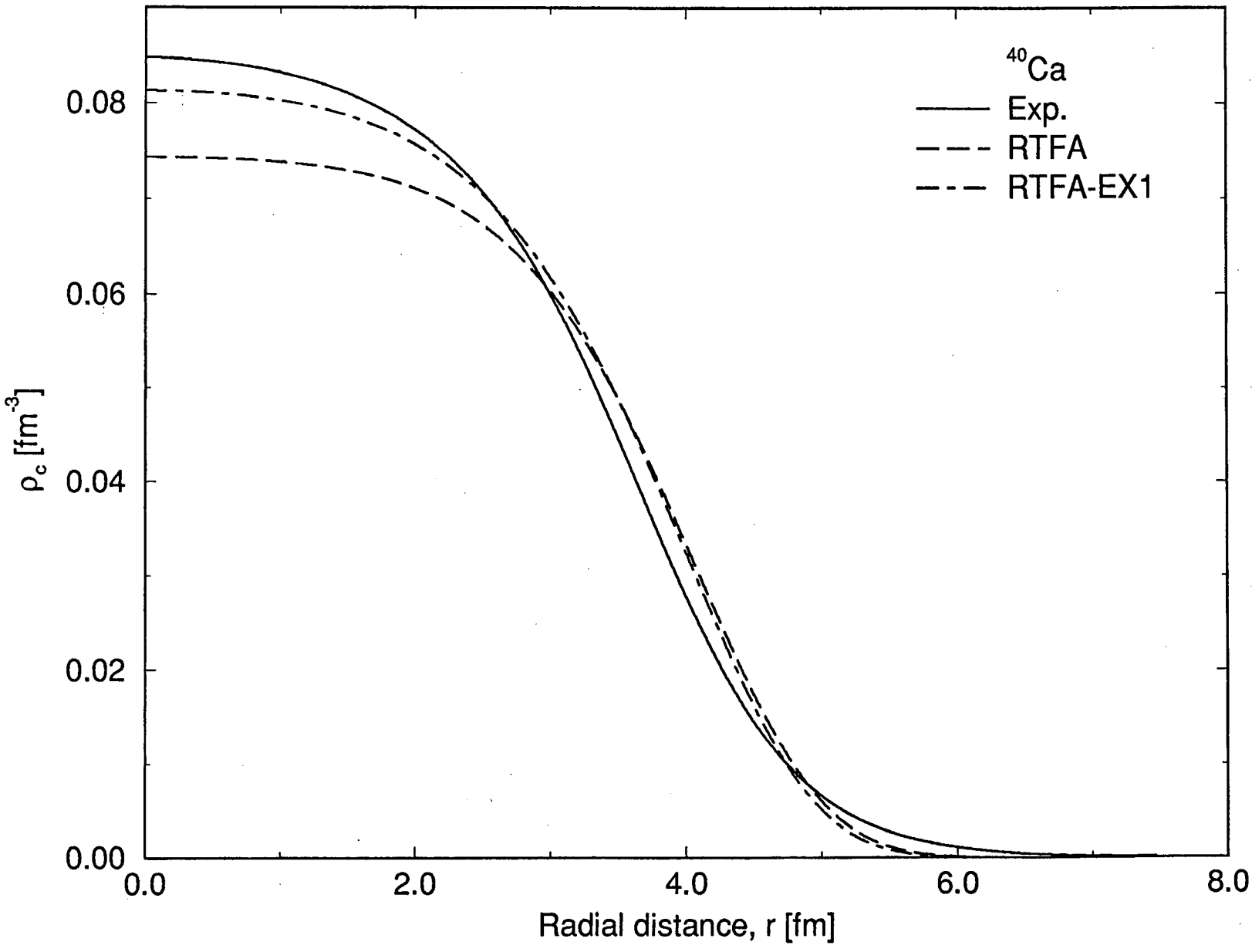
^{40}Ca
Exp.
RTFA
RTFA-EX1
0.08
0.06
0.04
0.02
0.00
ρ_c [fm^{-3}]
0.0
2.0
4.0
6.0
8.0
Radial distance, r [fm]

Fig.3

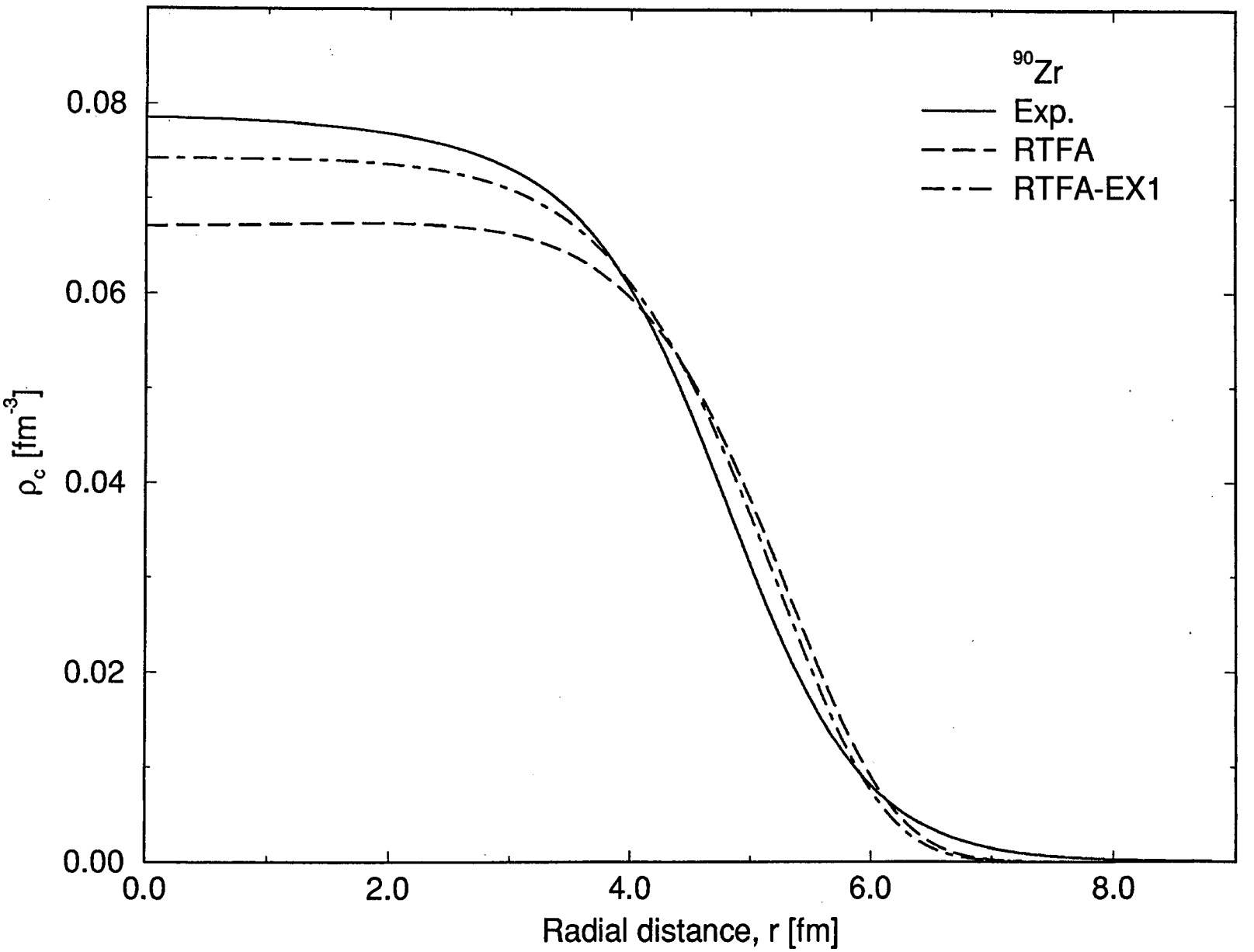
^{90}Zr
Exp.
RTFA
RTFA-EX1
0.08
0.06
0.04
0.02
0.00
ρ_c [fm^{-3}]
0.0
2.0
4.0
6.0
8.0
Radial distance, r [fm]

Fig.4

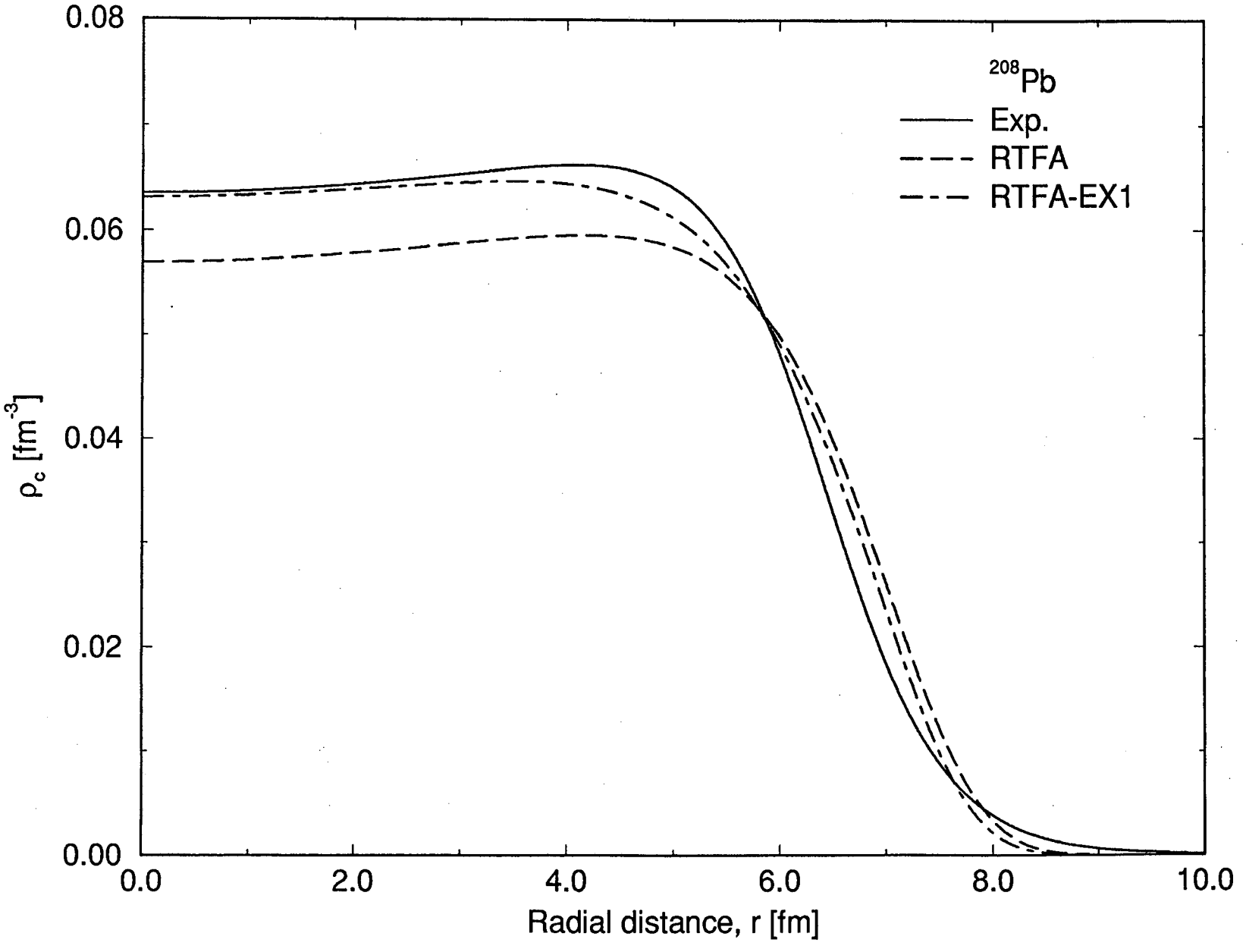
0.08
0.06
0.04
0.02
0.00
ρ_c [fm^{-3}]
0.0
2.0
4.0
6.0
8.0
10.0
Radial distance, r [fm]
^{208}Pb
Exp.
RTFA
RTFA-EX1

Fig.5

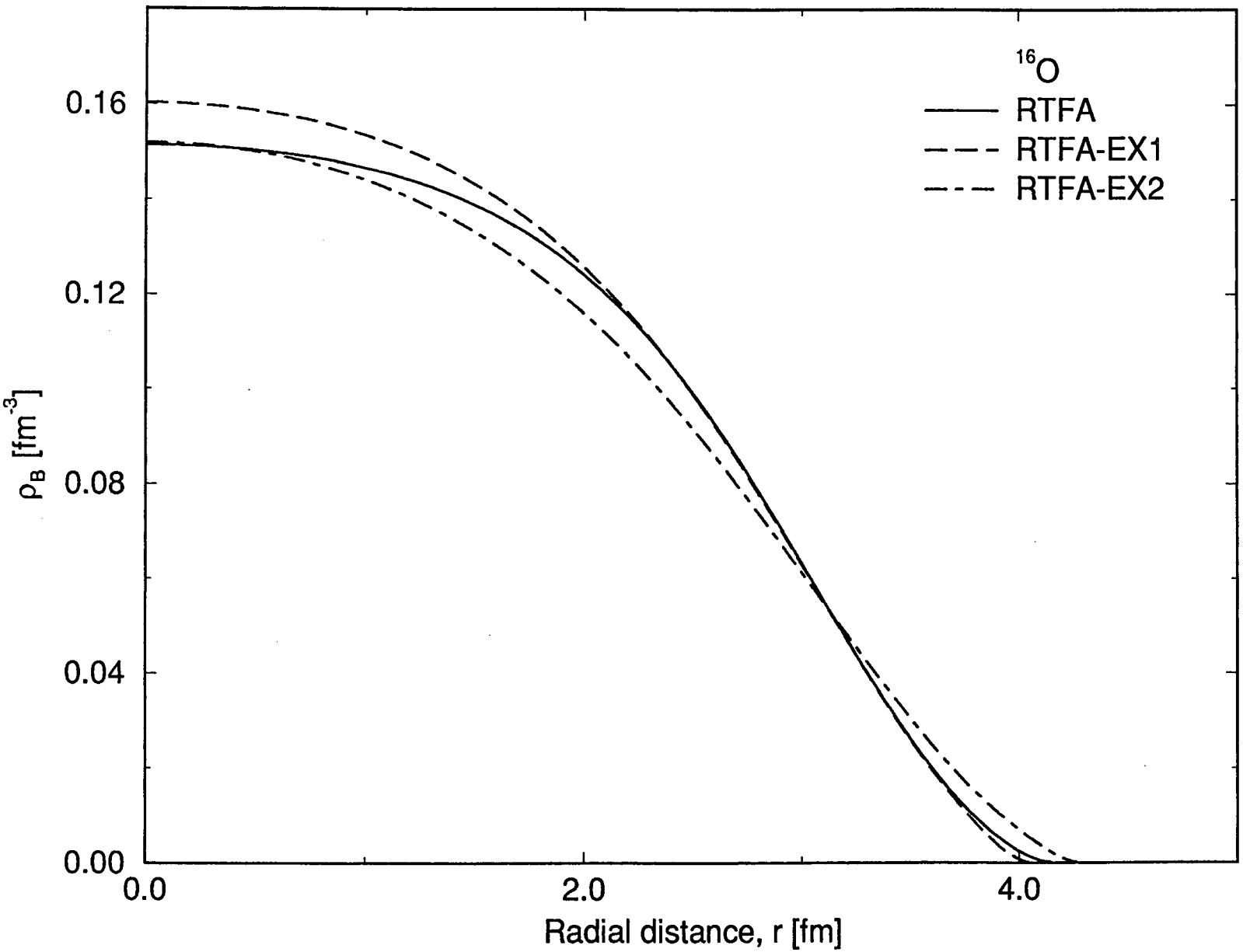
^{16}O
RTFA
RTFA-EX1
RTFA-EX2
0.16
0.12
0.08
0.04
0.00
ρ_B [fm^{-3}]
0.0
2.0
4.0
Radial distance, r [fm]

Fig.6

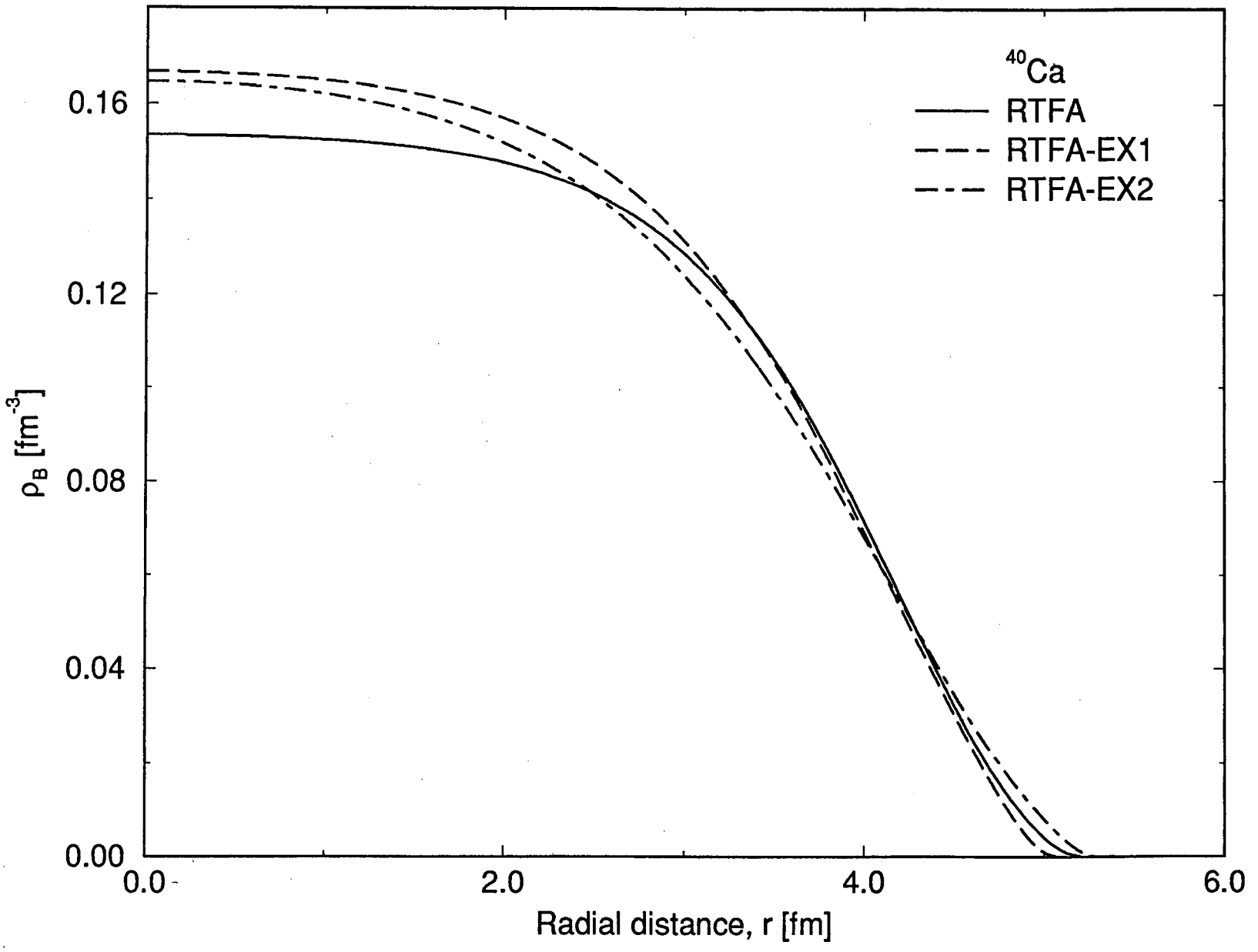
^{40}Ca
RTFA
RTFA-EX1
RTFA-EX2
0.16
0.12
0.08
0.04
0.00
ρ_B [fm^{-3}]
0.0
2.0
4.0
6.0
Radial distance, r [fm]

Fig.7

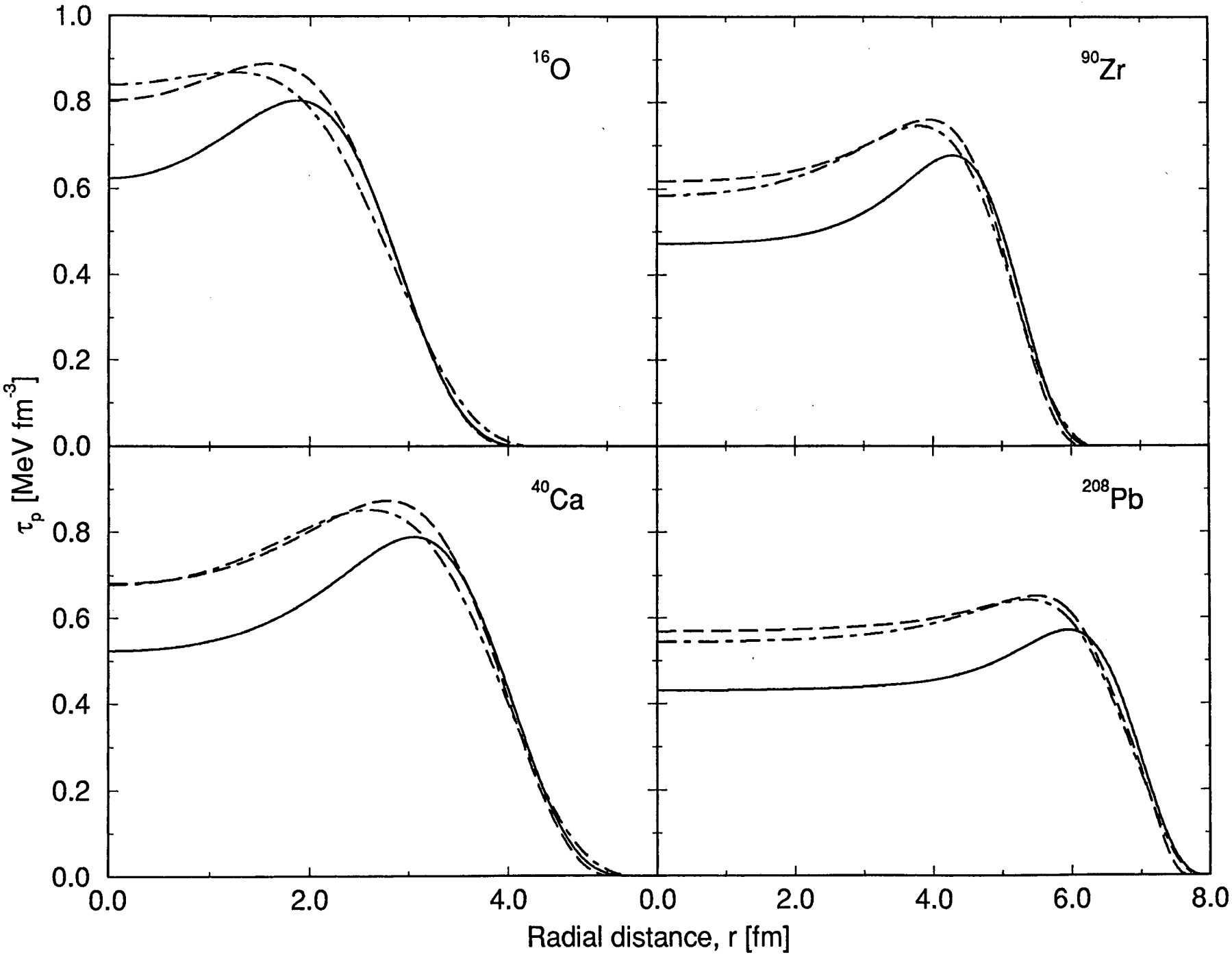
^{16}O
^{90}Zr
^{40}Ca
^{208}Pb
τ_p [MeV fm^{-3}]
Radial distance, r [fm]
0.0
0.2
0.4
0.6
0.8
1.0
2.0
4.0
6.0
8.0

Fig.8

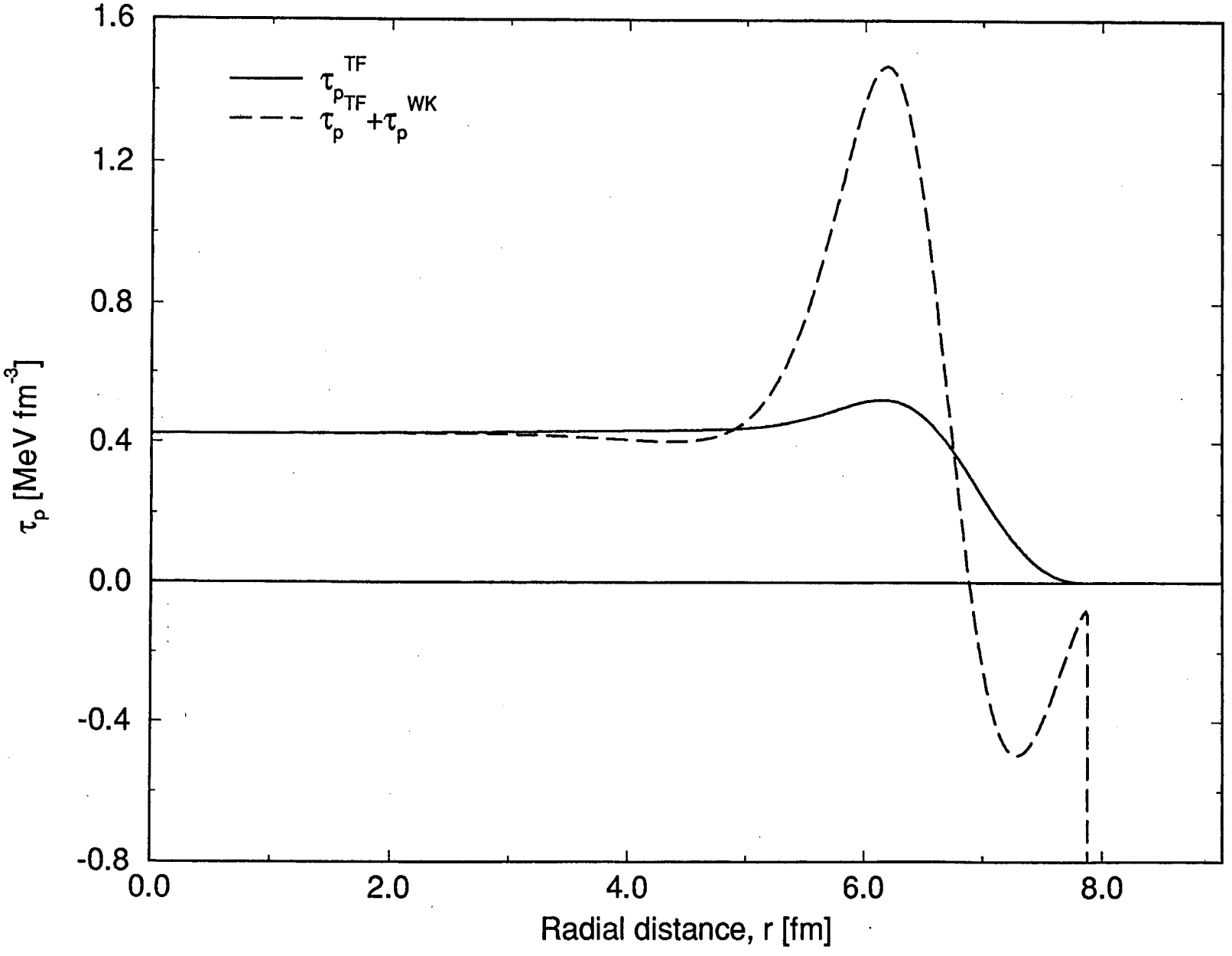
1.6
1.2
0.8
0.4
0.0
-0.4
-0.8
0.0
2.0
4.0
6.0
8.0
Radial distance, r [fm]
τ_p [MeV fm^{-3}]
τ_p^{TF}
$\tau_p^{TF}+\tau_p^{WK}$

Fig.9

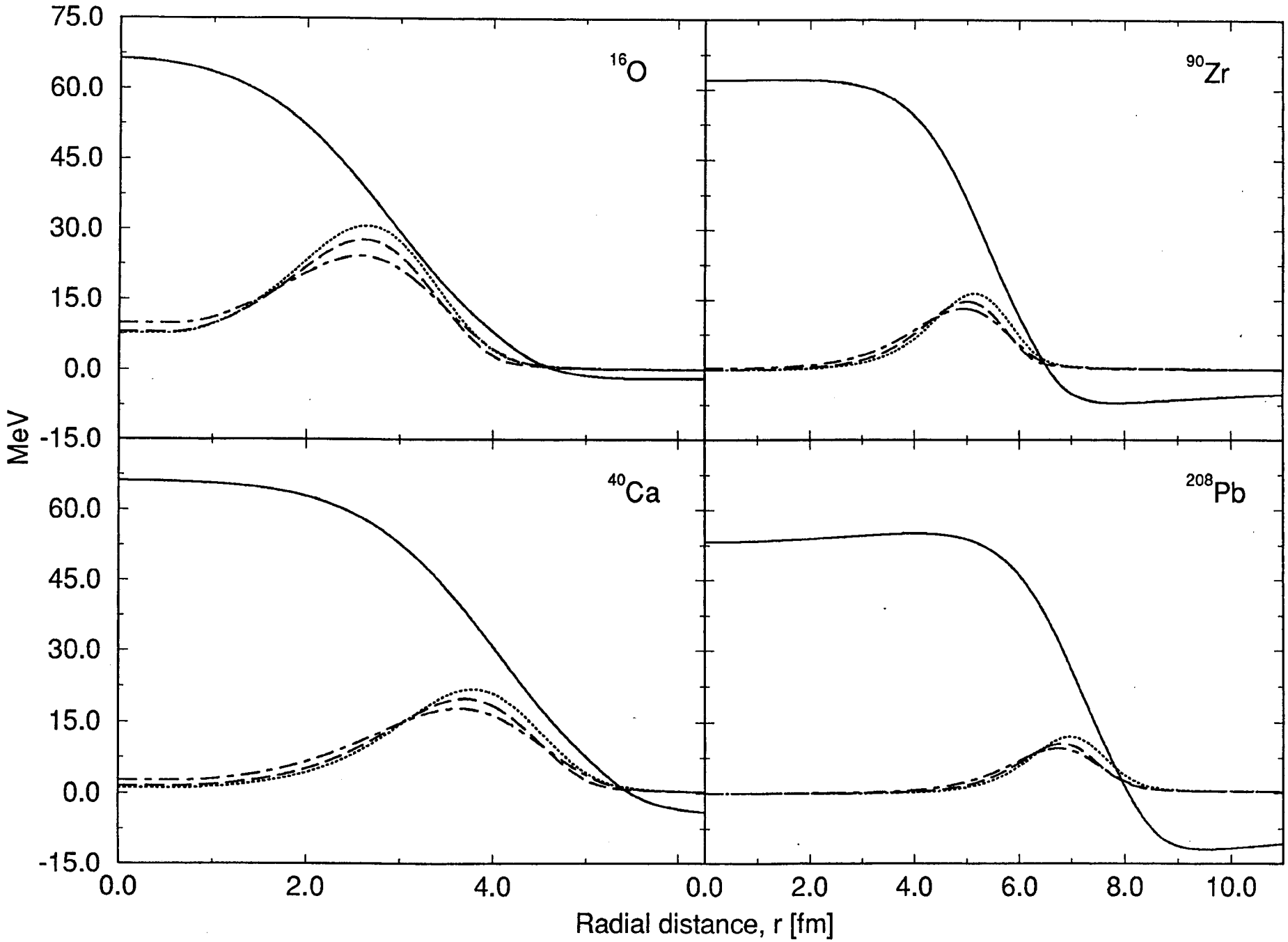
75.0
60.0
45.0
30.0
15.0
0.0
-15.0
MeV
^{16}O
^{90}Zr
^{40}Ca
^{208}Pb
0.0
2.0
4.0
6.0
8.0
10.0
Radial distance, r [fm]

LAWRENCE BERKELEY LABORATORY
UNIVERSITY OF CALIFORNIA
TECHNICAL INFORMATION DEPARTMENT
BERKELEY, CALIFORNIA 94720